KTH ROYAL INSTITUTE
OF TECHNOLOGY

Doctoral Thesis in Engineering Materials Science

Transition Metals and their Carbides, Nitrides and Carbonitrides

from a CALPHAD Perspective

FREDRIK HAGLÖF

Stockholm, Sweden 2021

Transition Metals and their Carbides, Nitrides and Carbonitrides

from a CALPHAD Perspective

FREDRIK HAGLÖF

Academic Dissertation which, with due permission of the KTH Royal Institute of Technology, is submitted for public defence for the Degree of Doctor of Philosophy on Monday the 20th December 2021, at 10:00 a.m. in Kollegiesalen, Brinellvägen 8, Stockholm.

Doctoral Thesis in Engineering Materials Science
KTH Royal Institute of Technology
Stockholm, Sweden 2021

© Fredrik Haglöf

ISBN 978-91-8040-087-9
TRITA-ITM-AVL 2021:51

Printed by: Universitetsservice US-AB, Sweden 2021

Abstract

The CALPHAD (CALculation of PHAse Diagrams) method consists of three cornerstones, i.e. experiments, computational methods (e.g. Density Functional Theory (DFT)) and thermodynamic models, which together are used to build CALPHAD descriptions. In this thesis the CALPHAD method, including all three parts, is used to study transition metals and their carbides, nitrides and carbonitrides. The focus is mainly on transition metals important for the steel and cemented carbide industries. Some of the weaknesses or uncertainties in existing thermodynamic descriptions of these transition metals are identified and investigated with either experiments or computational methods whereupon new descriptions are presented.

A method for calculation of the molar Gibbs energy as a function of temperature ($G_m(T)$) for metastable magnetic components is developed. The method uses DFT in combination with the Debye-Grüneisen model and the empirical magnetic model often used in CALPHAD. The developed method is also able to estimate the magnetic transition temperature (T_C or T_N). Furthermore, two new approaches for how to treat calculations on dynamically unstable allotropes are presented. This is important since this often is the reason why DFT calculations on metastable components fail. The method is developed and verified on bcc, fcc and hcp allotropes of Fe, Co and Ni, and is then used to calculate $G_m(T)$ descriptions for fcc-TiC, fcc-CrC, fcc-CrN, hcp-Cr_2C and hcp-Cr_2N. Furthermore, the same method is also used to calculate the excess Gibbs energy at 0 K for the interactions CrC-TiC (fcc), CrC-CrN (fcc) and Cr_2C-Cr_2N (hcp), as well as T_C and T_N as a function of composition for the same composition ranges.

Experiments are performed at 1673 and 1773 K to determine the solubility of Cr in MC (M = Ti, Cr) and of Ti in M_3C_2 and M_7C_3, in the equilibria MC-M_3C_2-M_7C_3 and MC-M_3C_2-graphite of the C-Cr-Ti system. The solubilities are measured with EDS/WDS and verified with XRD/Rietveld refinement.

The experimental and computational results for the C-Cr-Ti system are used together with literature data to perform a reassessment of this system. Compared to the previous CALPHAD description, the new description also includes updated descriptions for two of the three constituent binary systems (C-Ti and Cr-Ti) and reproduces the experimental results in the TiC-Cr_3C_2 isoplethal section found in literature.

In summary, the outcome of this thesis is an updated CALPHAD description of the C-Cr-Ti system and calculated $G_m(T)$ descriptions, including magnetic properties, for allotropes of Fe, Co, Ni, and several parameters in the C-Cr-N system. The developed method for calculation of $G_m(T)$ for metastable magnetic compounds is also a useful tool for calculation of $G_m(T)$ for many other transition metals and their carbides, nitrides, and carbonitrides.

Sammanfattning

CALPHAD (CALculation of PHAse Diagrams) metodiken består av tre hörnstenar, dvs. experiment, beräkningsmetoder (tex. Density Functional Theory (DFT)) och termodynamiska modeller, vilka tillsammans används för att skapa CALPHAD beskrivningar. I den här avhandlingen används CALPHAD metodiken, inklusive alla tre delar, för att studera övergångsmetaller och deras karbider, nitrider och karbonitrider. Fokuset ligger i huvudsak på övergångsmetaller som är viktiga inom stål- och hårdmetallindustrin. Några av svagheterna och osäkerheterna i befintliga thermodynamiska beskrivningar av dessa övergångsmetaller identifieras och undersöks med hjälp av antingen experiment eller beräkningsmetoder, varpå nya beskrivningar presenteras.

En metod för beräkning av den molära Gibbsenergin som funktion av temperatur ($G_m(T)$) för metastabila magnetiska komponenter utvecklas. Metoden använder DFT i kombination med Debye-Grüneisen-modellen och den empiriska magnetiska modellen som ofta används inom CALPHAD. Den utvecklade metoden kan också användas för att uppskatta den magnetiska omvandlingstemperaturen (T_C eller T_N). Dessutom presenteras två nya tillvägagångssätt för hur man ska behandla beräkningar på dynamiskt instabila komponenter. Detta är viktigt eftersom det ofta är anledningen till att DFT-beräkningar på metastabila komponenter misslyckas. Metoden utvecklas och verifieras på bcc-, fcc- och hcp-allotroper av Fe, Co och Ni, och används sedan för att beräkna $G_m(T)$ beskrivningar för fcc-TiC, fcc-CrC, fcc-CrN, hcp-Cr_2C och hcp-Cr_2N. Dessutom används samma metod också för att beräkna överskottet av Gibbs energi vid 0 K för interaktionerna CrC-TiC (fcc), CrC-CrN (fcc) och Cr_2C-Cr_2N (hcp), samt T_C och T_N som funktion av sammansättning för samma sammansättningsintervall.

Experiment utförs vid 1673 och 1773 K för att bestämma lösligheten av Cr i MC (M = Ti, Cr) och Ti i M_3C_2 och M_7C_3, i jämvikterna MC-M_3C_2-M_7C_3 och MC-M_3C_2-grafit i C-Cr-Ti-systemet. Lösligheterna mäts med EDS/WDS och verifieras med XRD/Rietveld-förfining.

De experimentella och beräknade resultaten för C-Cr-Ti-systemet används tillsammans med litteraturdata för att utföra en ny anpassning av detta system. Jämfört med den tidigare CALPHAD-beskrivningen innehåller den nya beskrivningen också uppdaterade beskrivningar för två av de tre ingående binära systemen (C-Ti och Cr-Ti) och reproducerar de experimentella resultaten i det isopleta snittet TiC-Cr_3C_2 som finns i litteraturen.

Sammanfattningsvis är resultatet av denna avhandling en uppdaterad CALPHAD-beskrivning av C-Cr-Ti-systemet och beräknade $G_m(T)$-beskrivningar, inklusive magnetiska egenskaper, för allotroper av Fe, Co, Ni och flera parametrar i C-Cr-N-systemet. Den utvecklade metoden för beräkning av $G_m(T)$ för metastabila magnetiska komponenter är också ett användbart verktyg för beräkning av $G_m(T)$ för många andra övergångsmetaller och deras karbider, nitrider och karbonitrider.

List of Papers

I ***Experimental study of carbides in the Ti−Cr−C system***
F. Haglöf, B. Kaplan, S. Norgren, A. Blomqvist, and M. Selleby
Journal of Material Science (2019) 54:12358–12370
Contribution statement: Fredrik performed the heat treatment (including furnace temperature calibration), performed sample preparation, EDS/WDS measurements, XRD measurements and Rietveld refinement, DFT calculations and prepared the manuscript.
Comment: The paper was nominated as *finalist to the 2019 Robert W. Cahn Best Paper Prize.*

II ***CALPHAD: Method for calculation of finite temperature thermodynamic properties for magnetic allotropes — Case study on Fe, Co and Ni***
F. Haglöf, A. Blomqvist, A. Ruban and M. Selleby
Calphad 74 (2021) 102320
Contribution statement: Fredrik performed the DFT calculations (including post-processing and method development) and prepared the manuscript.
Comment: The poster of this work received the *CALPHAD poster award* for one of the best posters presented at the CALPHAD GLOBAL Conference June, 2021.

III ***Thermodynamic assessment of the C−Cr−Ti system — Supported by DFT calculations***
F. Haglöf, A. Blomqvist and M. Selleby
Submitted to Calphad
Contribution statement: Fredrik performed the literature study, DFT calculations (including post-processing), the thermodynamic assessment and prepared the manuscript.

IV ***DFT study of the C−Cr−N system***
F. Haglöf, A. Blomqvist, and M. Selleby
In manuscript
Contribution statement: Fredrik performed the DFT calculations (including post-processing) and prepared the manuscript.

Other contributions by the author not included in the thesis.

A ***Solubility of Cr in Cubic Carbides***
F. Haglöf, B. Kaplan, S. Norgren, A. Blomqvist, and M. Selleby
Proceedings of the 19th Plansee Seminar, Reutte, Austria, 2017

B ***A third generation Calphad description of Fe: revisions of fcc, hcp and liquid***
Z. He, F. Haglöf, Q. Chen, A. Blomqvist, M. Selleby
In manuscript

Acknowledgement

When I finished my master many years ago, I was very tired of school and just wanted to start working. At that time PhD studies were not in my mind at all, and wasn't for a long time, until that day at the Sintering conference in Dresden when my colleague and supervisor, Susanne Norgren asked me if I shouldn't do PhD studies. Thank you very much Susanne for pushing me in the right direction!

Many thanks go to my main supervisor Malin Selleby for teaching me almost all I know about thermodynamic modelling and for always having answers for how to proceed in moments when I got stuck.

Thanks also to my supervisor Andreas Blomqvist, and early in my PhD studies also Bartek Kaplan, for introducing and teaching DFT to me. I would also like to thank Bartek for convincing me to use LaTeX instead of Word. Although I have many times struggled with LaTeX, it is a choice I have never regretted. I would also like to thank my co-author Andrei Ruban for introducing the Debye-Grüneisen model to me and for guiding me regarding magnetic DFT calculations.

Thanks to Wenli Long for teaching me how to use the SEM equipment, to Peter Hedström for valuable assistance with SEM and XRD and to Mikael Kritikos for valuable discussions about XRD and Rietveld refinement. Thanks to Zhangting He for valuable help with the third generation CALPHAD model and for all fruitful discussions about iron. Also thanks to Huahai Mao for valuable input about thermodynamic modelling, and especially regarding the assessment of C-Cr-Ti.

I would also like to thank Mari-Louise Englund, Juan Sandoval, Lars Tholander, Jonathan Chico and other past and present colleagues at Sandvik Coromant R&D and KTH. Many of you have helped me in different ways during my PhD studies, but unfortunately it is not possible to mention you all here. Thanks to my roommate at KTH, Adam Ståhlkrantz, and the other past and present PhD students at KTH, which I have had many interesting discussions with during the lunches and mini breaks in our PhD studies.

Furthermore, thanks to the Swedish Foundation for Strategic Research (SSF) for funding this project and to the Swedish National Infrastructure for Computing (SNIC) for providing computational resources for the DFT calculations.

Lastly, my warmest thanks go to my beloved wife Anna, and to my children Astrid and Axel. Without your understanding and support in times when I have been very occupied with work, this thesis would never have been possible.

Acronyms and symbols

AFM	Anti-ferromagnetic
bcc	Body-centred-cubic
CEF	Compound Energy Formalism
DFT	Density Functional Theory
DLM	Disordered Localized Moment
EDS	Energy-Dispersive X-ray Spectroscopy
fcc	Face-centred-cubic
FM	Ferromagnetic
hcp	Hexagonal-close-packed
NM	Non-magnetic
SEM	Scanning Electron Microscope
SQS	Special Quasirandom Structure
VASP	Vienna Ab-initio Simulation Package
WDS	Wavelength-Dispersive X-ray Spectroscopy
XRD	X-ray Diffraction
ZPE	Zero Point Energy

a	Lattice parameter
B_0	Bulk modulus
C_P	Isobaric heat capacity
d	Distance between lattice planes
E	Energy
E_0	Equilibrium energy
F	Helmholtz energy
G_m	Molar Gibbs energy
H	Enthalpy
$\mathbf{k}_B$	Boltzmann constant
l	Diffusion length
$n(\mathbf{r})$	Electron density as a function of spatial position (r)
$\mathbf{N}_A$	Avogadro constant
N_i	Number of moles of component i
$\mathbf{N}_u$	Number of atoms per formula unit

P	Pressure
$\mathbf{R}$	Molar gas constant
S	Entropy
t	Time
T	Temperature
$\mathbf{T}_C$	Curie temperature
$\mathbf{T}_N$	Néel temperature
$v(\mathbf{r})$	External potential as a function of spatial position (r)
V	Volume
V_0	Equilibrium volume
x_i	Mole fraction of component i
y_i	Site fraction of component i
β	Magnetic moment per atom
γ	Grüneisen parameter
θ	Diffraction angle
θ_D	Debye temperature
θ_E	Einstein temperature
λ	Wavelength

Contents

List of Papers iii

Acknowledgement v

Acronyms and symbols vii

Contents 1

1 Introduction 3
1.1 Background and scope of this thesis 4

2 Experimental methods 7
2.1 Sample synthesis 8
2.2 SEM, EDS and WDS 9
2.3 XRD and Rietveld refinement 11

3 Computational methods 15
3.1 DFT calculations 16
3.2 Harmonic and quasi-harmonic approximation 17
3.3 Debye-Grüneisen model 18
3.4 Dynamic instability 20
3.5 Electronic-, anharmonic- and vacancy contribution 21
3.6 Magnetic contribution 21
3.7 Disordered structures 23
3.8 Estimation of β, T_C and T_N 24

4 Thermodynamic modelling 27
4.1 Pure elements and stoichiometric compounds 27
4.2 Substitutional solution phases 28
4.3 Phases with sublattices 29
4.4 Metastable elements and compounds 31
4.5 Magnetic contribution to Gibbs energy 32

5 Summary of the included papers **37**
5.1 Paper I - Experimental study of carbides in the Ti–Cr–C system . . 37
5.2 Paper II - CALPHAD: Method for calculation of finite temperature thermodynamic properties for magnetic allotropes — Case study on Fe, Co and Ni 37
5.3 Paper III - Thermodynamic assessment of the C-Cr-Ti system — Supported by DFT calculations 38
5.4 Paper IV - DFT study of the C-Cr-N system 38

6 Concluding remarks **39**

7 Suggestions for future work **41**
7.1 C-Cr-N system 41
7.2 Method development 41

8 The 17 sustainable development goals **43**

References **45**

Chapter 1

Introduction

A common definition of the transition metals is that they represent the d-block, i.e. group 3-12, in the periodic table. However, sometimes the elements in group 3 and 12 are excluded as they exhibit different characteristic properties than the ones in group 4-11.

Many of the transition metals are essential in the materials industry, either as metals or as carbide-, nitride- and carbonitride formers, or both. The first example is, of course, Fe which is the base metal in the steel industry and hence need no further explanation. Fe also forms e.g. the carbide Fe_3C, which is known as cementite in steels. Other important transition metals in this industry are Cr and Ni, which mainly are added to improve the corrosion resistance. Many more transition metals (e.g. Mo, V, Co, Ti, Nb) are then used in order to give a steel different properties, e.g. to improve wear resistance, hot hardness, ductility, etc.

Another industry where transition metals are very important is the cemented carbide industry, where typically WC grains give hardness to the cemented carbide substrate and Co, as binder phase, contributes with toughness. Then many other transition metals are used to form different types of carbides, e.g. TiC, TaC, NbC and ZrC. Nitrides, e.g. TiN, and (TiAl)N, are also frequently used in this industry, either to improve hardness, e.g. in the coatings or in a cermet grade, or to create compositional gradients within the cemented carbide substrate. Also carbonitrides are often used, e.g. Ti(C,N), Ta(C,N) in order to improve the technological performance in some applications. Cr is nowadays also frequently used, as Cr has shown to be a very good grain growth inhibitor. Furthermore, also the interest for Fe and Ni has increased significantly in this industry the last decade. The reason for this is not mainly to improve the technological performance of the cemented carbide, but to be used as alternatives to Co as binder phase, as Co has shown to be carcinogenic when it is treated as a powder.

In this thesis different transition metals and their carbides, nitrides, and carbonitrides are studied using the CALPHAD (CALculation of PHAse Diagrams) method [1, 2]. The CALPHAD method consists of three cornerstones, i.e. exper-

iments, computational methods and thermodynamic models, which all three are necessary in order to build good CALPHAD descriptions. The CALPHAD descriptions can then be used in industry or academia to study stable and metastable equilibrium states. One example is to calculate the melting temperature and how it varies with composition. Other examples can be to calculate which phases are stable at a certain temperature, or to calculate the composition of a stable phase. Yet another useful application of a CALPHAD description is to calculate the driving force for precipitation of a phase.

Both in the steel and in the cemented carbide industry, the use of CALPHAD descriptions are very important. The main advantage is that it reduces the amount of needed experiments, since many properties can be predicted in advance. A typical example is to use a CALPHAD description to predict if a detrimental phase will be stable or not, e.g. the sigma phase in steel, or the eta phase or graphite in cemented carbides.

All three parts of the CALPHAD method are necessary. The experiments connects the description to reality and makes sure that the predictions are valid in the stable regions of the CALPHAD description. Computational methods, e.g. Density Functional Theory (DFT) calculations are needed to obtain better descriptions of metastable phases, which is essential in order to get more reliable extrapolations towards these regions. Finally the thermodynamic models are used to assess a CALPHAD description based on the information from experiments and the results from the computational methods. The strength with the thermodynamic models is then that, by using extrapolations, the CALPHAD description can be used to predict properties also at other conditions (e.g. compositions) than the description has been "trained" for. All three parts of CALPHAD are studied and used in this thesis.

1.1 Background and scope of this thesis

In the original plan for this thesis the aim was to use the CALPHAD approach to study nitrides and carbonitrides (but not carbides) of transition metals, starting with Cr, i.e. the C-Cr-N system. The plan further was then to add on other transition metals to the thermodynamic description, e.g. Ti, Al and W.

However, in the very beginning of this thesis work, recent experiments by He [3] and Ehrenborg [4] on the C-Cr-Ti system indicated that the modelled solubility of Cr in fcc-TiC in the existing thermodynamic description by Schuster and Du [5] were wrong. Furthermore, there were some concerns about if the heat treatment times used in their experiments [3, 4] were sufficient, why new experiments were needed. As the C-Cr-Ti system was planned to be part of the final outcome of this thesis, the decision was therefore to perform new experiments in the C-Cr-Ti system, which then also would work as a teaching system before the more complicated experiments on the C-Cr-N system were carried out. Experiments on N containing systems are difficult to perform since the partial pressure of N has to be controlled in some way,

either through a controlled furnace atmosphere or by enclosing the sample in an inert capsule.

The new experiments on the C-Cr-Ti system (**Paper I**) confirmed the indications by He [3] and Ehrenborg [4], that the thermodynamic description of the C-Cr-Ti system by Schuster and Du [5] had to be revised. The next planned step in this thesis was therefore to reassess the C-Cr-Ti system. The plan was further to use DFT to calculate $G_m(T)$ for fcc-CrC, as the description of this metastable end-member is a crucial parameter for describing the solubility of Cr in fcc-TiC. However, when the DFT calculations showed that fcc-CrC was ferromagnetic (FM), at 0 K, new questions arose. How is the magnetic transition temperature (T_C) calculated? And how can $G_m(T)$ above T_C, i.e. in the paramagnetic (PM) state, be described? Method development was therefore necessary, which were performed on allotropes of Fe, Co and Ni, and **Paper II** is the outcome of that work.

When it was clear how the magnetic properties from the DFT calculations should be treated in order to be translated to CALPHAD descriptions, fcc-CrC was calculated. The developed method was also used to calculate the molar excess Gibbs energy at 0 K, for the interaction in fcc (CrC−TiC) and the C-Cr-Ti system was then reassessed (**Paper III**).

First in **Paper IV** the focus was back on the C-Cr-N system. The built up knowledge about DFT and magnetism was used to calculate $G_m(T)$ for stable and metastable end-members in this system, but also to calculate the molar excess Gibbs energy at 0 K, for the interactions in fcc (CrC−CrN) and hcp (Cr_2C−Cr_2N).

Chapter 2

Experimental methods

In the CALPHAD approach, experiments is one of three cornerstones, besides computational methods (e.g. DFT) and thermodynamic modelling. By fitting model parameters to experimental data, the thermodynamic description can be considered as validated for the current conditions. There are many different experimental techniques that can be used to support CALPHAD modelling and by carefully selecting technique and design of the experiments a lot of information can be retrieved. One example of technique is melting point analysis, e.g. as Booker et al. [6] performed for varying compositions in the Ti-Cr-C system, results that were used for the thermodynamic assessment of the same system in this work (**Paper III**). Another example is measurements of the isobaric heat capacity ($C_P(T)$) of stable end-members, e.g. as Kelley [7] and Levinson [8] performed for fcc-TiC. This kind of measurements are very useful in a thermodynamic assessment since $C_P(T)$ is directly related to Gibbs energy ($G(T)$) as:

$$C_P(T) = -T \left(\frac{\partial^2 G(T)}{\partial T^2} \right)_P \tag{2.1}$$

Yet another example of useful experimental information is measurements of equilibrium pressure, e.g. measurements of the N_2 pressure as done for the bcc + hcp-Cr_2N and hcp-Cr_2N + fcc-CrN equilibria by Mills [9], which Frisk [10] then used in the thermodynamic assessment of the Cr-N system.

Finally, another common experimental technique is equilibrium heat treatments. With the right design of this type of experiment, i.e. selecting a total composition within a three phase equilibrium, one sample can give information about the phase compositions for all three phases, for the selected temperature. In this thesis this technique was used for measurements of equilibrium contents of Cr in fcc-TiC and Ti in the Cr_3C_2 and Cr_7C_3 carbides (**Paper I**). The following sections describe briefly the different steps of these types of equilibrium experiments.

2.1 Sample synthesis

The first step is to select type and amount of raw materials such that a desired overall composition is reached, e.g. within a supposed three phase region. Here, it can be wise to use two sets of raw materials, but with the same overall composition. If both samples end up with same results, it can then be assumed that they represent the equilibrium condition. The raw materials should then be mixed thoroughly. However, in order to minimize contamination of the powder, milling bodies should be avoided. After the mixing there are then two main alternatives:

1. **The powder is pressed or hot pressed at a temperature lower (or equal) to the succeeding heat treatment temperature** – The benefit with this alternative, which was used in **Paper I**, is that the grain sizes are kept rather small, close to the grain sizes of the raw materials. This means shorter diffusion paths and the time needed to reach equilibrium, in the succeeding heat treatment, is minimized. On the other hand, this method can result in porosity in the samples, which then instead might disturb the equilibration process.

2. **The powder is arc-melted** – The benefit with this alternative, which for example was used by He [3] and Ehrenborg [4], is less porosity, but the drawback is significantly larger grain sizes, and consequently the needed succeeding heat treatment time can increase drastically.

As discussed in **Paper I** it is quite possible that alternative 1 underestimates a solubility and alternative 2 overestimates it, e.g. as for Cr in fcc-TiC. Consequently, a good approach for this type of experiments would be to have one sample of each type for a selected overall composition. The sought solubility would then lie between the results of the two samples, but due to the shorter length of the diffusion paths in the hot pressed sample probably closer to this result. For the final step of the sample synthesis, the equilibrium heat treatment, there are four important parameters to consider:

1. **Furnace temperature** – Since the solubility limit for an element in a phase can vary significantly with temperature, e.g. as for Cr in fcc-TiC (**Paper I**), the furnace temperature has to be carefully calibrated before the heat treatment. This can for example be done using process temperature control rings (PTCR) or with samples of a pure element, which has a well-known melting temperature, as in **Paper I**, but it can also be done using external thermocouples.

2. **Furnace atmosphere** – The furnace atmosphere has to be selected such that the interaction with the samples is minimized. Often a good enough solution is to use an inert gas, e.g. Ar. However for N containing samples this would cause de-nitrification of the samples why an atmosphere with controlled partial pressure of N is needed. The easiest way to obtain this is to design

the sample powder with intended final N content and then enclose the sample in an inert capsule during the heat treatment. With this procedure, as e.g. Hertzman [11] used for experiments in the Fe-Cr-C-N system, reactions with the surrounding atmosphere can be avoided.

3. **Heat treatment time** − The heat treatment time has to be selected such that enough time is given for the sample to reach equilibrium. This time is very dependent on grain size, which determines the length of the diffusion paths, but also of the type of diffusing element. If the diffusion of a substitutional element is needed in order to reach equilibrium, e.g. Cr in **Paper I**, the needed heat treatment time will be much longer than if only diffusion of interstitial elements (e.g. C or N) is required. A rough estimation of the heat treatment time needed can be made with the Einstein equation for spherical cases:

$$l = \sqrt{6Dt} \tag{2.2}$$

where l is the diffusion length, which can be assumed to be the same as the typical grain size in the sample. D is the diffusion coefficient and here the smallest relevant D should be selected, as this corresponds to the limiting diffusion process. Finally, t is the time, which in this case is the wanted heat treatment time.

4. **Quenching or cooling** − The standard procedure for equilibrium heat treatment experiments is to quench the samples at the end of the heat treatment in order to freeze the equilibrium structure, i.e. to prevent kinetic driven processes to occur during cooling. For equilibrium experiments where diffusion of interstitial elements (e.g. C or N) are limiting, this is very important. However, this requires a special type of furnace with an attached quenching chamber. On the other hand, for equilibrium experiments where diffusion of substitutional elements are limiting, e.g. Cr in the C-Cr-Ti samples in **Paper I**, the heat treatment times can be very long, e.g. 300 h in **Paper I**. In these cases it is sufficient to use a furnace with fast cooling, e.g. 10 K/min, which enables use also of other types of heat treatment furnaces.

2.2 SEM, EDS and WDS

After the heat treatment it is time to analyse the phase compositions. Here it is recommended to use two independent methods. Preferably Energy Dispersive X-ray Spectroscopy (EDS) or Wavelength Dispersive X-ray Spectroscopy (WDS) in combination with X-ray diffraction (XRD). XRD will be further discussed in the next section (Sec. 2.3). The reason to use two methods is that with EDS/WDS the composition of each phase can be measured, but there is no information retrieved about the crystallographic structure of the phase. With XRD, on the other hand, it is more or less the opposite. If the system is rather well known, e.g. as the C-Cr-Ti system in **Paper I**, there are probably no doubts about the crystallographic

structures, but it can still be a good idea to use both methods. Hence, if XRD is used in combination with Rietveld refinement [12], also the phase compositions can be estimated, why this method is useful for verifying the EDS/WDS results, e.g. as done in **Paper I**.

For both EDS and WDS, a scanning electron microscope (SEM) is used. Detailed information about SEM, EDS and WDS, can be found in the extensive book by Goldstein et al. [13]. Here only a short introduction to the topic will be presented followed by comments on important parameters that were considered when using EDS and WDS for phase analysis in the present work (**Paper I)**.

The SEM used in this thesis was equipped with a tungsten filament, which under high current emits electrons that are used to bombard the sample. This result in many types of signals from the sample, secondary electrons (SE), back-scattered electrons (BSE) and X-rays. By scanning the sample and using detectors for SE or BSE, images of the sample can be created. Fig. 2.1 shows an example of a BSE image from **Paper I**. In BSE images phases with heavier elements are brighter, because these elements render more backscattered electrons.

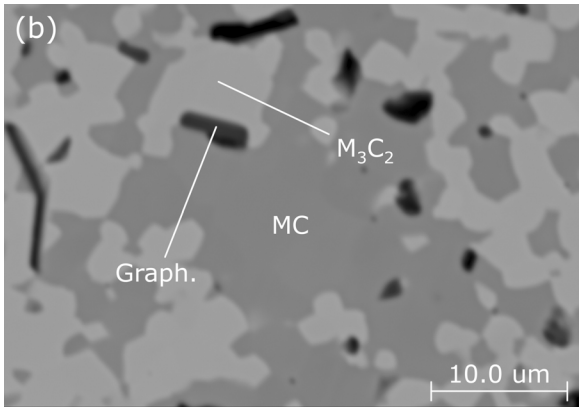

Figure 2.1: Example from **Paper I**. Back-scattered electron (BSE) image showing the microstructure of a sample in the MC-M_3C_2-graphite equilibrium (M=Ti,Cr).

To do phase analysis with EDS or WDS, the sample is bombarded at a single spot, i.e. in the phase of interest. This creates SE and BSE but what is of interest here is the X-rays emitted when electrons from outer electron shells fall to inner shells in order to fill the gaps from excited electrons. The EDS detector analyses the energy of the emitted X-rays to determine their origin, i.e. which element they stem from. However, there are two main drawbacks with EDS. One is that very light elements, e.g. as C or N cannot be detected and the second is that the energy peaks are overlapping for some elements, why it can be difficult to distinguish between these elements.

With WDS the emitted X-rays from the sample passes a crystal which only lets X-rays with a certain wavelength pass. With this procedure only the X-rays,

which belongs to a chosen element will reach the WDS detector. The advantage is that light elements can be studied with this technique, but also that energy peaks are much narrower, why it is easier to distinguish between different elements. The drawback is that the WDS detector can measure only one element at the time, why these measurements are very time consuming. There are equipments, e.g. Electron Probe Micro Analyzer (EPMA), which have more than one WDS detector and therefore can analyse several elements simultaneously, but unfortunately the one used in **Paper I** only had one detector.

There are some important things to consider when using EDS or WDS:

1. As the amount of emitted X-rays can vary over time, e.g. caused by a drift in the beam current, the system should be calibrated regularly during the measurements. The calibration can be performed with measurements on a piece of pure Cu.

2. Standards with a well-known composition (as close as possible to the measured phase), should be used as reference for the measurements. This is especially important for the WDS measurements, but also good for EDS. The standards should be treated as equally as possible as the samples, e.g. if the samples are coated with a conductive layer of C, the standards should be too, and so on.

3. The size of the measured grains should be large enough to avoid interaction with neighbouring grains. The interaction volume the electron beam creates is mainly dependent on the composition of the measured grain and the acceleration voltage used for the electron beam. The interaction volume can be estimated with a Monte Carlo simulation. Fig. 2.2 is an example from **Paper I**, which shows a Monte Carlo simulation of electron trajectories in solid TiC, using the software Casino v2.51, an acceleration voltage of 15 kV and an assumed beam diameter of 100 nm.

4. Measurements should be made on many different grains for each phase. The main reason is that the composition can vary between grains, why many measurements are needed to get a statistically better average, but also to retrieve a standard deviation for the phase composition. Another reason is that if a measured grain is very shallow, the measurement can partly represent the grain beneath the measured grain. With many measurements, these shallow grains can probably be identified as outliers and be excluded.

2.3 XRD and Rietveld refinement

Similar to SEM, a tungsten filament is used in XRD to create a beam of electrons. However, in XRD the electrons are not used to bombard the sample, but instead to bombard a known element in order to produce X-rays with a specific wavelength.

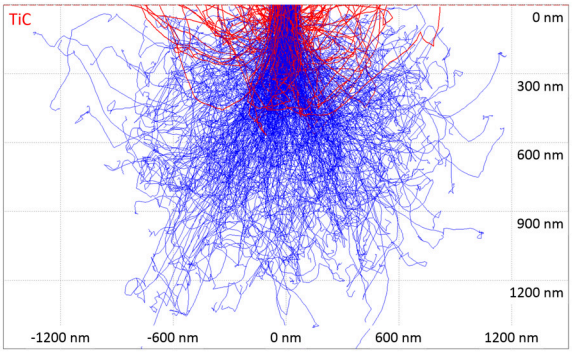

Figure 2.2: Example from **Paper I**. Monte Carlo simulation of electron trajectories in solid TiC (red lines = backscattered electrons, blue lines = X-rays). Acceleration voltage = 15 kV, beam diameter = 100 nm.

The element can be Co, Cr, Fe or Mo, but the most commonly used is Cu, which also was used in this thesis (**Paper I**). A reason to change element is if the sample of interest has reflections overlapping with Cu. The generated X-rays are then used to hit the sample from a range of different angles (θ), as Fig. 2.3 shows.

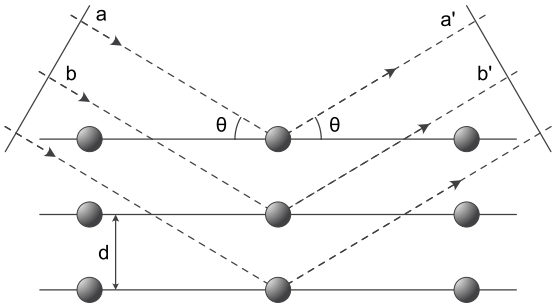

Figure 2.3: Schematic figure of how X-rays are diffracted by a crystal.

Reflections are obtained when θ in combination with the distance (d) between two lattice planes is such that the travelled distance for the diffracted X-ray b' is exactly one wavelength (or a multiple thereof) longer than the distance travelled by a'. The θ for which reflections are retrieved can be calculated with Bragg's law:

$$n\lambda = 2dsin(\theta) \tag{2.3}$$

where n is an integer multiple and λ is the wavelength, which is known. Each crystallographic structure then have more than one type of lattice planes, why the structure generates a characteristic pattern of reflections as a function of θ, which can be used to identify the crystal structure for a phase. As the distance between

lattice planes in a crystal structure is dependent on the elements it contains, also the composition can be estimated. One example is the calculated amount of Cr in fcc-TiC in **Paper I**. In that case DFT where used to calculate the lattice parameter as a function of Cr content in fcc-(Cr,Ti)C. Rietveld refinement [12] of the retrieved XRD-pattern were then used to find the actual lattice parameter of fcc-(Cr,Ti)C in the sample, which then could be translated to a composition using Vegard's law [14].

In a Rietveld refinement [12], a software is used (e.g. PANalytical HighScore Plus 3.0d as in this thesis) to match a measured XRD pattern to one or several reference patterns of known structures. The software creates a calculated XRD pattern from the selected reference patterns and if the patterns match, it can be assumed that the correct phases have been identified. However, the reference patterns are normally pure compounds, and the phases in the sample are probably not pure, why the measured peaks can be slightly shifted to other θ, due to somewhat different d. What Rietveld refinement [12] then does, is to let the software adjust the lattice parameters of the reference patterns to get an even better fit. There are then even more parameters that can be optimized in a Rietveld refinement [12], e.g. peak shape, specimen displacement and atomic positions in the lattice. When a good fit is retrieved the calculated XRD pattern matches all peaks in the measured XRD pattern. Fig. 2.4 shows an example of a Rietveld refined [12] XRD pattern from **Paper I**, which contains the phases fcc-MC, M_3C_2 and M_7C_3 (M=Cr,Ti).

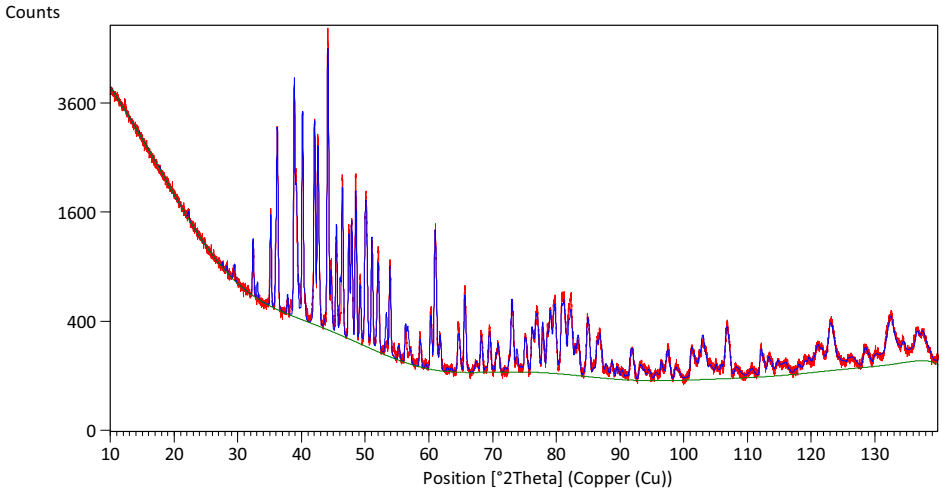

Figure 2.4: Example from **Paper I**. XRD pattern of a sample containing the phases fcc-MC, M_3C_2 and M_7C_3 (M=Cr,Ti). Calculated diffraction pattern using the Rietveld refined phase structures (blue) compared with the measured diffraction pattern (red).

When an XRD pattern is used for Rietveld refinement [12] it is important to use a sufficiently long measurement time at each θ. There is always background noise during the measurement, which gives reflections at all θ, and if the measured time at each θ is too short, important peaks might drown in this background noise. It is also important to make sure that the measurements cover all θ of interest. This was missed in **Paper I**, where the first measurements were started at $2\theta = 30°$. But as the characteristic peak for graphite is below this value, the retrieved XRD patterns gave no information about if the sample contained graphite or not, why new measurements were needed. Further reading about the XRD technique can be found in the book by Suryanarayana and Norton [15].

Chapter 3

Computational methods

The second of three cornerstones in CALPHAD is the use of computational methods (e.g. DFT) to estimate thermodynamic properties of metastable compounds, as experiments on these compounds are difficult to perform. The only possibility to do experiments on metastable compounds is to, in some way, force the compound to be stable. However, since some constraints then have been introduced, it can be questioned if these experiments really can represent the metastable equilibrium. Two examples are the measurements of magnetic properties on fcc-Fe precipitates in a fcc-Cu matrix by Gonser et al. [16] and on bcc-Ni layers on GaAs(001) by Tian et al. [17], which are further discussed in **Paper II**. A better alternative is to retrieve a property by extrapolation from stable compositions of the phase, e.g. as Ohno [18] did in order to retrieve the magnetic properties for hcp-Fe. However, these type of extrapolations assume that no transition (e.g. in magnetic configuration) occurs in the metastable region, which might not be true. This is also further discussed in **Paper II**.

It is for these reasons that DFT and other computational methods, e.g. the Debye-Grüneisen method [19, 20], come to use, as equilibrium properties can be calculated for any type of compound and magnetic configuration without introducing any further constraints. However, the results are dependent on that the models and approximations used in these methods are accurate enough for the current compound, which is not always the case. Due to this, the results should be handled with care and, as far as possible, the results should be verified with calculations on similar, but stable compounds, where experimental information is available. This is the background to the method development in **Paper II**, but also the reason why verifying calculations were performed on the stable compounds fcc-TiC in **Paper III**, and fcc-CrN and hcp-Cr_2N in **Paper IV**. Another concern with the computational methods is that, since any magnetic configuration can be calculated, many different possibilities have to be tested in order to find the configuration with the lowest energy, e.g. as for the Fe, Co and Ni allotropes in **Paper II** and the Cr containing compounds in **Paper III** and **Paper IV**. However, there is always some

remaining uncertainty whether there exists another magnetic configuration with lower energy, which has not been tested.

3.1 DFT calculations

The physics and theories behind DFT calculations have not been the main focus in this thesis work. Instead focus has been on the use of DFT from a CALPHAD perspective, which in this thesis means to:

1. Identify important parameters in a CALPHAD description, which cannot be determined experimentally.
2. Use well-known DFT methods combined with the Debye-Grüneisen model and if necessary also develop new methods to calculate these parameters.
3. Verify the methods used with calculations on similar, but stable, compounds where experimental information is available.
4. Compare the results with existing thermodynamic descriptions found in literature.
5. Translate the calculated properties to a format that can be used in a CALPHAD description.

However, it can be of interest to briefly describe the background of DFT and how the method works, why a short summary is here presented. Density functional theory (DFT) is, as the name implies, a theory based on functionals (i.e. functions of other functions) of the electron density, $n(\mathbf{r})$, where $\mathbf{r}$ is a spatial position. By using this theory, properties for a system with many electrons, e.g. an atom or a compound, can be calculated. In principle these properties can be calculated with quantum mechanics by solving the Schrödinger equation for many atoms, $\mathcal{H}\psi = E\psi$, where E is the energy and ψ is the wave function. The problem is that this requires to calculate the Hamiltonian ($\mathcal{H}$), which includes five different types of contributions, the electrostatic nucleus-nucleus, nucleus-electron and electron-electron interactions as well as the kinetic energies of the nuclei and electrons, where each type can consist of a very large number of interactions and kinetic energies (depending on the size of the system). Therefore, this partial differential equation is far too complex to be solved.

However, within DFT some assumptions and simplifications have been introduced, which makes the equation solvable. The Born-Oppenheimer approximation [21] assumes that the electrons move much faster than the nuclei and that the system therefore can be treated as stationary nuclei surrounded by an electron cloud. The nucleus-nucleus interactions and the kinetic energy of the nuclei can thus be neglected. This simplified the problem, but it was still too complex. Hohenberg and Kohn [22] then came with their theorem for an electron gas:

"... that there exists a universal functional $F[n(\mathbf{r})]$ independent on the external potential $v(\mathbf{r})$, such that the expression $E \equiv \int v(\mathbf{r})n(\mathbf{r})d\mathbf{r}+F[n(\mathbf{r})]$ has its minimum value, the correct ground state energy, associated with $v(\mathbf{r})$".

As they also proved that the external potential ($v(\mathbf{r})$) is uniquely defined if $n(\mathbf{r})$ is known, the correct ground state can thus be found by minimizing $E[n]$, but Hohenberg and Kohn [22] did not have the full solution how to do it. This remaining link to the solution was instead presented by Kohn and Sham [23]. They simplified the problem by assuming that the system could be treated as a hypothetical system of non-interacting electrons that generate the same electron density as the real system. This results in Schrödinger-like equations, but they are much simpler to solve as the effective external potential then only is dependent on one electron. If the functional $F[n(\mathbf{r})]$ in the expression by Hohenberg-Kohn [22] is extended, E as a functional of n can then be expressed as:

$$E[n] = T_s[n] + \int v(\mathbf{r})n(\mathbf{r})d\mathbf{r} + E_H[n] + E_{xc}[n] \tag{3.1}$$

where $T_s[n]$ is the kinetic energy of the hypothetical non-interacting electron system, the second term corresponds to the electrostatic nucleus-electron interaction, $E_H[n]$ is the Hartree energy (or Coloumb energy i.e. the energy for the electrostatic electron-electron interaction) and $E_{xc}[n]$ is a remaining exchange correlation energy for electron-electron interactions. This made it possible to find the ground state, by minimizing $E[n]$, as Hohenberg-Kohn [22] predicted. However, as $v(\mathbf{r})$ is dependent on $n(\mathbf{r})$ this has to be done iteratively, but there are many software packages available that solves this problem.

In this thesis, all DFT calculations were performed using the Vienna Ab initio Simulation Package (VASP) [24, 25] together with the projector augmented wave (PAW) potentials [26, 27] and the exchange-correlation functional used was the Perdew-Burke-Ernzerhof (PBE) [28] version of the generalized gradient approximation (GGA).

Finally, there are some DFT input parameters which are important in order to retrieve sensible results and have therefore been carefully converged in this thesis. These parameters are mainly the sampling mesh of the Brillouin zone (i.e. the number of k-points), the energy cut-off for the plane waves (*ENCUT*) and the size of the special quasi-random structure (SQS) supercells. These parameters are dependent on structure, included elements, system size, etc., why they have to be converged in every single case. The parameters used have therefore been specified for each case in **Paper I-IV**.

3.2 Harmonic and quasi-harmonic approximation

For CALPHAD purposes, the simplest case is to use DFT to estimate the Enthalpy of formation ($\Delta_f^\circ H_m^\phi$) at 0 K for a compound. This is often done by assuming that vibrational (phonon) contributions can be neglected at 0 K even if this is not fully

true, there is vibrational energy also at 0 K, i.e. the zero point energy (ZPE). Anyhow, with this assumption, Helmholtz energy (F) for the equilibrium volume (V_0) is equal to $E_{stat}(V_0)$, which is the static energy at 0 K and can be retrieved from a DFT calculation. As $G = F + PV$, where P is pressure and V is volume and $G = H - TS$, where both the temperature (T) and the entropy (S) are 0, $\Delta_f^\circ H_m^\phi$ can then be calculated, e.g. as for Ti_7C_3 in **Paper III**:

$$\Delta_f^\circ H_m^{Ti_7C_3} = H_m^{Ti_7C_3} - 7H_m^{hcp-Ti} - 3H_m^{graph.-C} \tag{3.2}$$

By also including the vibrational contribution at 0 K, a better estimation of $\Delta_f^\circ H_m^\phi$ can then be made. Furthermore, if also V and T dependent vibrational, and other contributions are added to F, also thermodynamic properties at finite temperatures can be estimated. By including the configurational entropy ($S_{conf}(V,T)$), which is 0 for pure elements and stoichiometric compounds, the expression for $F(V,T)$ is also valid for disordered phases and can be expressed:

$$\begin{aligned} F(V,T) = {} & E_{stat}(V) + E_{vib}(V,T) - T\left[S_{vib}(V,T) + S_{conf}(V,T) + S_{mag}(V,T)\right] \\ & + F_{el}(V,T) + F_{anh}(V,T) + F_{vac}(V,T) \end{aligned} \tag{3.3}$$

where $E_{vib}(V,T)$ and $S_{vib}(V,T)$ are the vibrational contribution to energy and entropy, respectively and $S_{mag}(V,T)$ is the magnetic entropy. Energy contributions from electronic excitations, anharmonic vibrations and thermal vacancies are described by $F_{el}(V,T)$, $F_{anh}(V,T)$ and $F_{vac}(V,T)$, respectively.

By adding T dependent vibrational contributions calculated at only V_0, a harmonic approximation of $F(V,T)$ is retrieved. This can be done by performing a harmonic phonon calculation, e.g. using the VASP integrated Phonopy package [29, 30]. This approximation assumes that the equilibrium volume is independent on T. As for example Fig. 3.1 shows for fcc-Co, this is not true, as the equilibrium volume increases with T. If also V dependence is included for $E_{vib}(V,T)$ and $S_{vib}(V,T)$, a quasi-harmonic approximation is retrieved. This can be obtained by performing harmonic phonon calculations for several different V and then minimize $F(V,T)$ with respect to V at each T (Fig. 3.1). Another possibility to obtain a quasi-harmonic approximation, which has been used in this thesis, is to use the Debye-Grüneisen model [19, 20], which will be further explained in Sec. 3.3.

3.3 Debye-Grüneisen model

A quasi-harmonic approximation of F can also be made with the Debye-Grüneisen model [19, 20], which was used in this thesis. The method is described in detail in **Paper II** and will therefore here only be presented briefly.

The first step is to fit a DFT calculated E-V curve at 0 K to the Birch-Murnaghan equation of state [31, 32]:

$$E(V) = E_0 + \frac{9V_0B_0}{16}\left\{\left[\left(\frac{V_0}{V}\right)^{\frac{2}{3}} - 1\right]^3 B_0' + \left[\left(\frac{V_0}{V}\right)^{\frac{2}{3}} - 1\right]^2\left[6 - 4\left(\frac{V_0}{V}\right)^{\frac{2}{3}}\right]\right\} \tag{3.4}$$

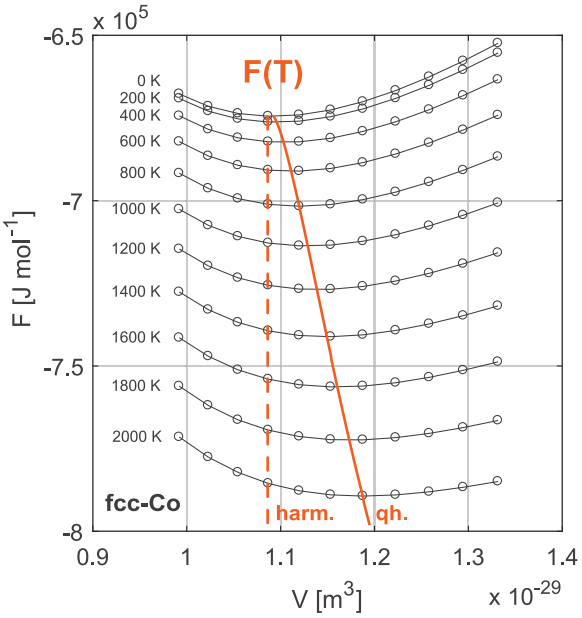

Figure 3.1: $F(V)$, for a number of different T, for fcc-Co. The diagram also shows how F varies with T, when using the harmonic (harm., orange dashed line) and quasi-harmonic (qh., orange solid line) approximations.

The equilibrium energy at 0 K (E_0), the equilibrium volume at 0 K (V_0), the bulk modulus (B_0), and the derivative of the bulk modulus (B_0') are then retrieved, where $E_{stat}(V_0)$ in Eq. 3.3 then is equal to E_0. According to the Debye theory [19], $E_{vib}(V,T)$ and $S_{vib}(V,T)$ (Eq. 3.3) can be calculated as:

$$E_{vib}(V,T) = \frac{9}{8} N_U N_A k_B \theta_D(V) + 3 N_U N_A k_B T D\left(\frac{\theta_D(V)}{T}\right) \tag{3.5}$$

$$S_{vib}(V,T) = 3 N_U N_A k_B \left\{ \frac{4}{3} D\left(\frac{\theta_D(V)}{T}\right) - ln\left[1 - exp\left(-\frac{\theta_D(V)}{T}\right)\right]\right\} \tag{3.6}$$

where N_U is the number of atoms per formula unit, N_A is the Avogadro constant, k_B is the Boltzmann constant, $D(x)$ is the Debye-function and $\theta_D(V)$ is the volume dependent Debye temperature. $\theta_D(V)$ can be calculated from the Debye temperature at equilibrium volume at 0 K ($\theta_D(V_0)$) as:

$$\theta_D(V) = \theta_D(V_0)\left(\frac{V_0}{V}\right)^{\gamma} \tag{3.7}$$

where γ is the Grüneisen parameter [20]. According to Moruzzi et al. [33] $\theta_D(V_0)$ can be approximated using a function which includes B_0, V_0 and a constant s,

which they called a *scaling factor*. However, Chen and Sundman [34] showed that this s is not constant, but in fact can vary between different compounds, why the method by Moruzzi et al. [33] to calculate $\theta_D(V_0)$ can be questioned. In this thesis $\theta_D(V_0)$ was instead calculated from the vibrational energy at 0 K, the zero point energy ($ZPE(V_0)$):

$$\theta_D(V_0) = \frac{8}{9}\frac{ZPE(V_0)}{N_U N_A k_B} \tag{3.8}$$

where $ZPE(V_0)$ can be retrieved from a harmonic phonon calculation, which in this thesis was made with the VASP integrated Phonopy package [29, 30] together with the density functional perturbation theory (DFPT) [35].

The final parameter needed to be able to calculate $E_{vib}(V,T)$ and $S_{vib}(V,T)$ (Eqs. 3.5 and 3.6) is then γ (Eq. 3.7), which can be calculated using the general formula as presented by Zharkov et al. [36]:

$$\gamma = -\frac{V}{2}\frac{\frac{\partial^2 P}{\partial V^2} - \frac{2m}{3}\left(\frac{2m}{3}+1\right)\frac{P}{V^2}}{\frac{2m}{3}\frac{P}{V} + \frac{\partial P}{\partial V}} - \frac{m+2}{3} \tag{3.9}$$

where the approximation by Dugdale-MacDonald [37] ($m = 1$) was used in this thesis. The pressure (P) can be derived from the Birch-Murnaghan equation of state (Eq. 3.4) as $P(V) = -\frac{\partial E(V)}{\partial V}$ and then also the pressure derivatives ($\frac{\partial P}{\partial V}$ and $\frac{\partial^2 P}{\partial V^2}$) can easily be calculated.

3.4 Dynamic instability

The classical quasi-harmonic approximation (Sec. 3.2) requires that harmonic phonon calculations are performed for several different V. However, if the compound is dynamically unstable for any of the needed V, phonon calculations using 0 K methods, e.g. using Phonopy [29, 30, 35], for this V is not reliable and the method fails.

One advantage with the Debye-Grüneisen model, in the way it has been used in this thesis (Sec. 3.3), is that as long as the structure is dynamically stable at V_0, $\theta_D(V_0)$ can be calculated (Eq. 3.8) and a quasi-harmonic approximation of F can be retrieved. As a matter of fact, as long as the structure is dynamically stable at any V, the Debye-Grüneisen model (Sec. 3.3) can be used, since $\theta_D(V_0)$ then can be calculated from $\theta_D(V)$ using Eq. 3.7. This method was for example used for bcc-Ni in **Paper II**.

However, even if the structure is dynamically unstable at all V, a thermodynamic description of the compound is still needed in a CALPHAD description. Due to this a new method was developed in **Paper II**, which extrapolates $ZPE(V_0)$ from β-values, where $ZPE(V_0, \beta)$ is dynamically stable, to retrieve $ZPE(V_0)$ for the equlibrium β (i.e. $ZPE(V_0, \beta_{Eq.})$). This method was validated for bcc-Fe and then used for bcc-Co, as Fig. 3.2 shows.

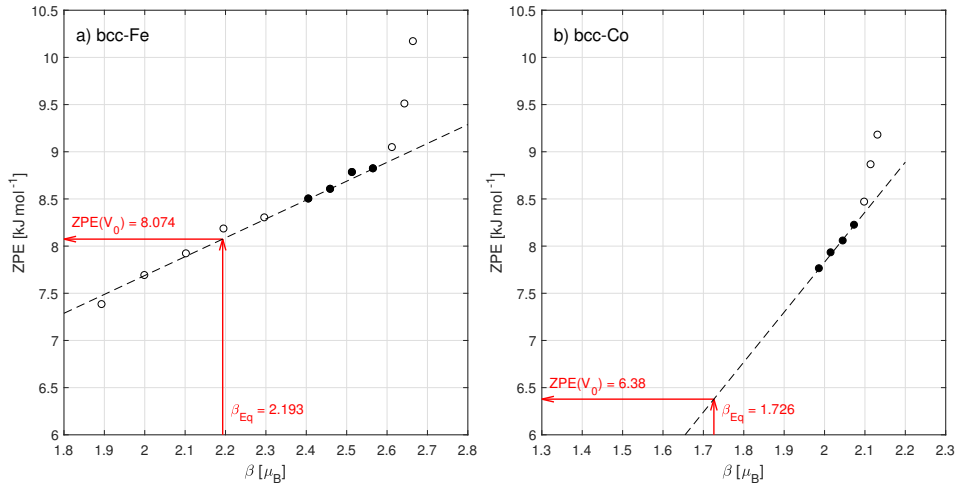

Figure 3.2: Example from **Paper II**. Calculated zero point energy (ZPE) as a function of magnetic moment per atom (β) for the equilibrium volume (V_0) for a) bcc-Fe and b) bcc-Co. Dashed lines are fitted to points with filled markers.

3.5 Electronic-, anharmonic- and vacancy contribution

Of the final three contributions to $F(V,T)$ (Eq. 3.3), only the energy contribution due to electronic excitations ($F_{el}(V,T)$) has been included in this thesis. This contribution has been calculated by performing static DFT calculations for a grid of different V and T, using Fermi smearing in VASP, as explained in more detail in **Paper II**. As an example, Fig. 3.3 shows the calculated $F_{el}(V,T)$ for fcc-CrC, from **Paper III**.

Furthermore, the quasi-harmonic approximation assumes that the atoms vibrate symmetrically. This is in general not true, i.e. there is also a contribution from anharmonic vibrations ($F_{anh}(V,T)$). At higher temperatures there is also an energy contribution due to the formation of vacant positions in the lattice, i.e. thermal vacancies ($F_{vac}(V,T)$). Glensk et al. [38] and Grabowski et al. [39] showed that both contributions can be calculated within the framework of DFT. However, these contributions are relatively small and the effort needed to calculate them is rather large, which is further discussed in **Paper II**, why neither $F_{anh}(V,T)$ nor $F_{vac}(V,T)$ have been included in this thesis.

3.6 Magnetic contribution

Several transition metal compounds (e.g. the bcc, fcc and hcp allotropes of Fe, Co and Ni) undergoes a magnetic transition at some critical temperature. For compounds that are ferromagnetic (FM) at low temperatures, which means their

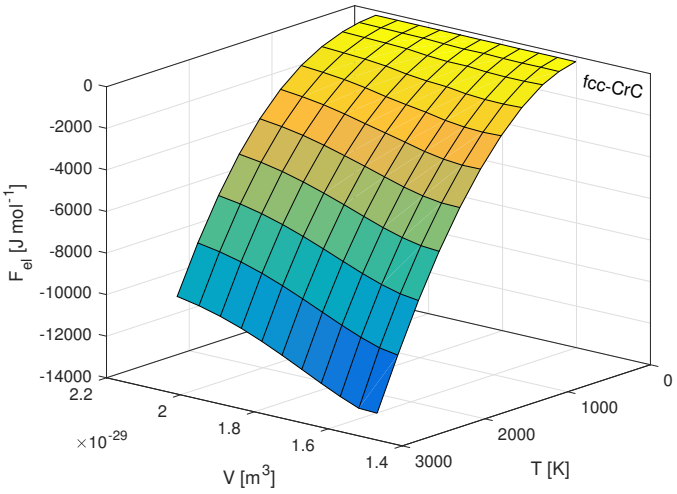

Figure 3.3: Calculated $F_{el}(V,T)$ per formula unit of fcc-CrC.

atoms have magnetic spin aligned in the same direction, the magnetic transition temperature is called the Curie temperature (T_C). For anti-ferromagnetic materials (AFM), half the number of atoms have spin in one direction and the other half in the opposite direction, in an ordered arrangement, why the total magnetic moment is zero. However, as this ordering can be configured in many different ways, there are several possible AFM configurations. Fig. 3.4 is an example from **Paper II**, which shows three different types of AFM structures in hcp. The AFM-II structure is for example the magnetic ground state structure for hcp-Fe, according to this thesis (**Paper II**), which is also in agreement with Bigdeli et al. [40]. Furthermore, an AFM structure can also be even more complex. One example is the magnetic structure for fcc-Fe, which according to experiments by Tsunoda [41] is a spin-density-wave. This structure was later studied with DFT by Sjöstedt and Nordström [42] and Marsman and Hafner [43], and was also studied in this thesis when searching for the magnetic ground state structure of fcc-Fe (**Paper II**). Another example is the magnetic structure of bcc-Cr which was reported by Corliss et al. [44] to be even more complex. Different type of AFM structures are further discussed and evaluated for each type of compound in **Paper II and IV**. For AFM materials the magnetic transition temperature is called the Néel temperature (T_N).

Above the critical temperature all these materials (FM and AFM) are paramagnetic (PM), in which all atoms still have magnetic spin, but the direction of the magnetic spins are totally random. For the PM structure this randomness creates a magnetic entropy (S_{mag}), which is the obvious magnetic contribution to $F(V,T)$ (Eq. 3.3). According to Grimvall [45] S_{mag} can be calculated as:

$$S_{mag} = Rln(2S_a + 1) \tag{3.10}$$

where S_a is the magnetic spin per atom. However, also the other contributions to $F(V,T)$ (Eq. 3.3) are dependent on the magnetic structure (FM, AFM or PM), why these have to be calculated using spin-polarized calculations in VASP [24, 25]. For spin-spiral structures also non-collinearity has to be included in the calculations, as the spins are not aligned. However, if calculated ground state energies are to be compared between different structures, they have to be calculated with the same method, why non-collinearity has to be accounted for, for all structures, if a spin-spiral is one of the candidates. This was shown to be important for fcc-Fe in **Paper II**.

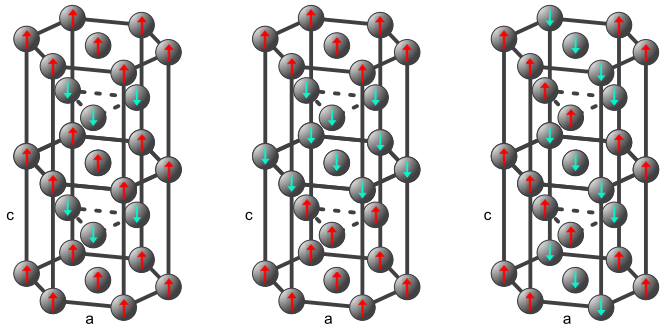

Figure 3.4: Example from **Paper II**. Antiferromagnetic structures in hcp: AFM-I, AFM-D and AFM-II. Arrows represent the direction of the magnetic spin, i.e spin up (red) and spin down (cyan)

3.7 Disordered structures

To use DFT to calculate the energy for a disordered structure, e.g. fcc-(Ti,Cr)C (mixed carbide), hcp-Cr_2(C,N) (carbonitride) or to estimate the PM energy for a magnetic compound, a special quasirandom structure (SQS) supercell SQS [46–48] can be used. The SQS cell is much larger than the cells used for ordered structures, since a certain number of atoms have to be included in order to represent a random arrangement of the atoms. To estimate the PM state, SQS can be used together with the disordered local moment (DLM) approach [49, 50]. In the DLM-SQS cell half the number of atoms, randomly distributed, are assigned with an initial spin up and the other half with spin down. Fig. 3.5 shows an example from **Paper IV** with both disordered composition (carbonitride) and disordered magnetic spin (DLM). The phase is fcc-Cr(C,N) with a site fraction of N, $y_N = 0.167$ (18 of 108 atoms on the second sublattice). On the first sublattice, 54 Cr atoms are assigned with spin up and 54 Cr atoms with spin down, randomly distributed.

However, during the electronic relaxation, i.e. the DFT calculation, there is a risk that the magnetic spin for some of the atoms change sign and the initial ran-

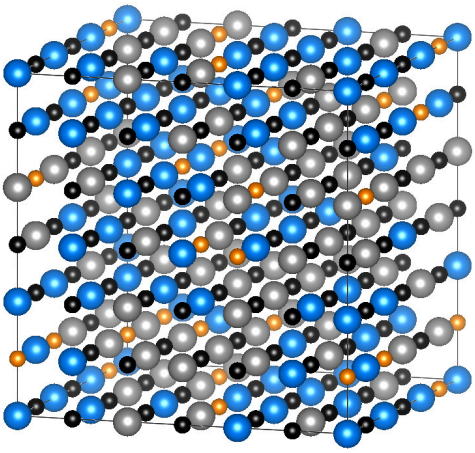

Figure 3.5: One of the DLM-SQS cells of fcc-Cr(C,N) used in **Paper IV**. First sublattice: 54 Cr atoms with spin up (grey) and 54 Cr atoms with spin down (blue). Second sublattice: 90 C atoms (black) and 18 N atoms (orange).

domness is destroyed. This risk is even more pronounced if the magnetic moments (β) are small. After a DLM-SQS calculation it is therefore important to check that the initial signs of the magnetic spins have not changed during the relaxation. If this turns out to be a problem, this can be handled with a special method developed in this thesis work (**Paper II**). By setting the initial β to a fix value for each atom, the initial randomness can be kept during the relaxation. However, as the equilibrium β for the DLM structure is not known, it is then necessary to repeat the calculation for many different β, in order to find the minimum energy. Furthermore, the lattice parameter for the DLM structure is also not known in advance, even if a good guess is that it is similar to the lattice parameter for the corresponding ordered magnetic structure. It is rather time consuming to relax the lattice parameter for a cell with many atoms, why it instead can be more efficient to perform static DFT calculations, i.e. only relaxing the electronic structure, for several different volumes. In order to find the equilibrium state for the DLM-SQS structure it is therefore necessary to perform calculations for a grid of different lattice parameters and β values as Fig. 3.6 shows.

3.8 Estimation of β, T_C and T_N

To avoid describing the ordered magnetic state (FM or AFM) and the paramagnetic state as two different phases in a CALPHAD description an empirical magnetic model that describes the magnetic transition has instead been implemented. This magnetic model, which is further explained in Sec. 4.5, requires that β and T_C/T_N are known. β can be retrieved from the DFT calculation at the equilibrium volume

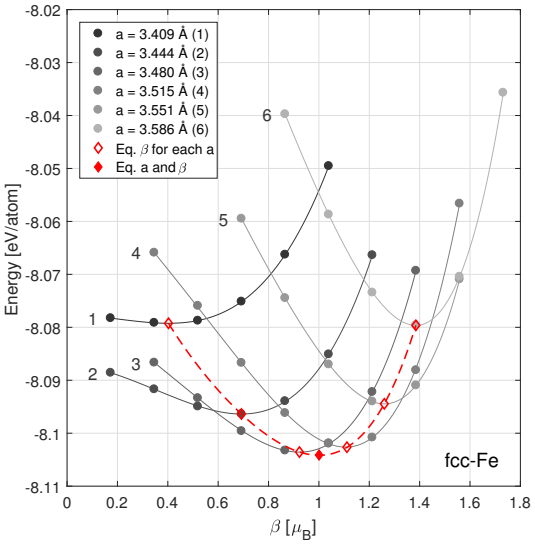

Figure 3.6: Example from **Paper II**. Calculated DLM energy/atom as a function of magnetic moment per atom (β) for different lattice parameters (a) for fcc-Fe. Red unfilled diamonds represent equilibrium β for each a and the red filled diamond represents equilibrium β for the equilibrium a.

of the ordered magnetic structure. However, for the AFM structures the total magnetic moment is zero, but each atom still has a magnetic moment. β can then be estimated to be the same as is presented for each atom in the *OUTCAR* file from VASP. However, this β is calculated within the defined sphere of the atom, and since spheres are not able to fill out the full volume, without overlap, this value is not fully correct. A better way, if possible, is to calculate the AFM structure as a spin spiral. A total magnetic moment for the cell is then retrieved, and a more correct β can be calculated. This method was used for the AFM allotropes in **Paper II**, where it also is explained how a temperature dependent β can be retrieved, if necessary.

To calculate T_C/T_N using DFT is not trivial, and there is no known method that has been proven to work in general. However, within CALPHAD a more pragmatic approach can be used, which does not need to be physically explained. With the empirical magnetic model used in CALPHAD, the energy difference between FM/AFM and the PM structure at 0 K can be calculated if β and T_C/T_N are known. On the other hand, this also means that if this energy difference and β are known, T_C/T_N can be calculated. In this thesis it was found that if the energy for the PM state is calculated as the average of the energy for the stable ordered magnetic state (FM or AFM) and the DLM-SQS energy, this method gives reasonable values for T_C/T_N for in principle all allotropes of Fe, Co and Ni (**Paper II**). Therefore this method was used also in **Paper III** and **Paper IV**.

Chapter 4

Thermodynamic modelling

The final of three cornerstones in CALPHAD is the thermodynamic modelling, where the strength lies in the ability to predict thermodynamic properties also in higher order systems by extrapolation. The CALPHAD method is based on the concept of finding the equilibrium state for a specified condition, i.e. pressure (P), temperature (T) and composition (N_i, i.e number of moles of component i). Gibbs energy (G) for a phase (ϕ) can be expressed as a function of these state variables, i.e. $G(P, T, N_i)$, why the equilibrium state at each given condition (P, T, N_i) is found as the phase, or combination of phases, that gives the lowest G. Another advantage with G is that all other thermodynamic properties, e.g. enthalpy (H), entropy (S) and heat capacity (C_P), can be calculated if G is known. When G for different phases are to be compared the amount of the phases has to be the same, why G for a phase often is expressed for one mole of atoms, i.e. the molar Gibbs energy (G_m). The total G_m of a phase (ϕ) can then be expressed as [51]:

$$G_m^\phi = {}^{srf}G_m^\phi - T \cdot {}^{conf}S_m^\phi + {}^{phys}G_m^\phi + {}^{E}G_m^\phi \tag{4.1}$$

where ${}^{srf}G_m^\phi$ represents the surface of reference, which is a linear combination of G_m^ϕ of the constituents of the phase. T is the temperature and ${}^{conf}S_m^\phi$ is the configurational entropy, which is added in order to describe the energy contribution due to ideal mixing of the constituents of the phase. However, in reality most phases deviate from the ideal behaviour and therefore an excess Gibbs energy term is added (${}^{E}G_m^\phi$). Furthermore, there can also be contributions from other physical phenomena (${}^{phys}G_m^\phi$), where magnetism is the most common one. The magnetic contribution will be further described in Sec. 4.5.

4.1 Pure elements and stoichiometric compounds

To be able to calculate ${}^{srf}G_m^\phi$ a description of the molar Gibbs energy as a function of temperature ($G_m^\phi(T)$) of all constituents (end-members) of the phase are needed. For stable allotropes of pure elements or stoichiometric compounds there is often

sufficient experimental information available to base the $G_m^\phi(T)$ description on. $G_m^\phi(T)$ can in these cases be modelled as [51]:

$$^\circ G_m^\phi(T) - \sum_i a_i H_i^{SER} = A + BT + CTln(T) + DT^2 + ET^{-1} + FT^3 \qquad (4.2)$$

where ϕ is the phase (e.g. fcc), a_i is the stoichiometric factor of element i in ϕ (e.g. $a_{Cr} = 1$ in fcc-CrN), H_i^{SER} is the enthalpy of element i in its standard reference state (SER), which usually is the stable state at 298.15 K. A, B,... F are constants. The superscript $^\circ$ on $^\circ G_m^\phi(T)$ indicates that the description is representing a pure component.

This model represents the second generation of CALPHAD descriptions. However, due to the $CTln(T)$ and ET^{-1} terms this model is not able to correctly describe $^\circ G_m^\phi(T)$ down to 0 K. Consequently CALPHAD descriptions that use this second generation $^\circ G_m^\phi(T)$ descriptions are normally only valid above room temperature (298.15 K). On the other hand, for many applications this limitation is not critical.

In the third generation CALPHAD descriptions a more physically based model is used, i.e. a function based on the Einstein temperature (θ_E) [52–54]. With this model the polynomial function is much shorter, usually only two terms are needed, and the $^\circ G_m^\phi(T)$ descriptions are valid down to 0 K:

$$\begin{aligned} &^\circ G_m^\phi(T) - \sum_i a_i H_i^{SER} = \\ &\quad E_0 + \frac{3}{2}R\theta_E + 3RT \times ln\left[1 - exp\left(-\frac{\theta_E}{T}\right)\right] + AT^2 + BT^n + ... \end{aligned} \qquad (4.3)$$

where E_0 is the equilibrium energy at 0 K and R is the molar gas constant. Of course it is preferred to use the third generation model, especially in new CALPHAD descriptions. However, this requires that θ_E is given for all end-members in the CALPHAD description. Consequently, if the aim with the retrieved $^\circ G_m^\phi(T)$ description is to update an existing CALPHAD description, the second generation model must be used.

4.2 Substitutional solution phases

The substitutional solution model is used to describe $G_m(T)$ for phases where all constituents can substitute for each other because they all occupy the same lattice sites. This model is typically used to describe both the gas phase and the liquid phase. In its simple form, which applies to the liquid phase, the constituents are assumed to be the same as the components. $G_m(T)$ can therefore be expressed using mole fractions (x_i) of the components i:

$$G_m^\phi = \sum_i x_i {}^\circ G_i^\phi + RT \sum_i x_i ln(x_i) + {}^E G_m^\phi \qquad (4.4)$$

where ${}^{\circ}G_i^{\phi}$ is the molar Gibbs energy of the pure component i in ϕ. The first term represents ${}^{srf}G_m^{\phi}$, the second term corresponds to ${}^{conf}S_m^{\phi}$ and the last term represents ${}^{E}G_m^{\phi}$ in Eq. 4.1. ${}^{E}G_m^{\phi}$ can then be expanded to:

$$ {}^{E}G_m^{\phi} = \sum_i \sum_{j>i} x_i x_j I_{i,j}^{\phi} + \sum_i \sum_{j>i} \sum_{k>j} x_i x_j x_k I_{i,j,k}^{\phi} + ... \tag{4.5} $$

where each $I_{i,j}^{\phi}$ represents a binary interaction parameter, which modelled with a Redlich-Kister polynomial [55] can be expressed as:

$$ I_{i,j}^{\phi} = \sum_{n=0}^{q} {}^{n}L_{i,j}^{\phi}(x_i - x_j)^n \tag{4.6} $$

where q represents the total number of interaction parameters, ${}^{n}L_{i,j}^{\phi}$. If q=0 we only have an ${}^{0}L$ parameter and the model is called a regular solution. With q=1 we also get an ${}^{1}L$ parameter and it is then called a sub-regular solution. With yet another L parameter it will be a sub-sub-regular solution and so on. Furthermore, all ${}^{n}L_{i,j}^{\phi}$ can be linearly dependent on T:

$$ {}^{n}L_{i,j}^{\phi} = {}^{n}a + {}^{n}bT \tag{4.7} $$

The last term in Eq. 4.5 represents the ternary part of ${}^{E}G_m^{\phi}$, where the interaction parameter ($I_{i,j,k}^{\phi}$) can be modelled with composition dependence, preferably with the model suggested by Hillert [56]:

$$ I_{i,j,k}^{\phi} = \nu_i {}^{0}L_{i,j,k}^{\phi} + \nu_j {}^{1}L_{i,j,k}^{\phi} + \nu_k {}^{2}L_{i,j,k}^{\phi} \tag{4.8} $$

Also here each ${}^{n}L_{i,j,k}^{\phi}$ can be linearly dependent on T (similar to Eq. 4.7) and the ν fractions are calculated as:

$$ \nu_i = x_i + (1 - x_i - x_j - x_k)/3 \tag{4.9} $$

$$ \nu_j = x_j + (1 - x_i - x_j - x_k)/3 \tag{4.10} $$

$$ \nu_k = x_k + (1 - x_i - x_j - x_k)/3 \tag{4.11} $$

In this thesis work the substitutional solution model was used to describe the liquid phase for the C-Cr-Ti system (**Paper III**).

4.3 Phases with sublattices

As described in the previous section the substitutional solution phase has only one sublattice. However, there are many cases where the components have preferential

sites in the lattice, why it is necessary to model these phases with two, or even more, sublattices. One typical example is when smaller atoms (e.g. C and N) prefer to occupy interstitial sites and larger atoms (e.g. the transition metals) prefer the substitutional sites in a lattice. It is then natural to model such phase with two sublattices, one for the substitutional atoms and one for the interstitial atoms. A typical model for this type of phase would then be expressed:

$$(M_1, M_2, M_3, ...)_a(X_1, X_2, ...)_b \tag{4.12}$$

where each M_i represents a substitutional element, each X_i is an interstitial soluble element and a and b are the number of sites for each sublattice. By including vacancies (Va), e.g. as one of the X, this model is also capable to describe a situation when some of the interstitial sites are un-occupied. The common phases, bcc, fcc and hcp, are usually modelled this way. Furthermore, these phases are normally modelled with one site (a=1) for the substitutional sublattice, and the number of interstitial sites (b) will then be 3, 1 and 0.5 for bcc, fcc and hcp, respectively.

The first sublattice model, which included two sublattices with only two constituents on each sublattice, was presented by Hillert and Staffansson [57]. The model was then extended, first by Harvig [58] to include an arbitrary number of constituents on each sublattice, and then by Sundman and Ågren [59] to include an arbitrary number of sublattices. The sublattice model [57–59] is the base for the compound energy formalism (CEF), which is described in more detail by Hillert [60]. The composition range for a phase with sublattices is limited by the composition of its extremities (end-members) of the phase, i.e. the cases when each sublattice is fully occupied with only one constituent. CEF is based on the assumption that these end-members (compounds) can be used to describe the surface of reference (${}^{srf}G_m^{\phi}$), which is needed to calculate the total Gibbs energy for a phase (Eq. 4.1). With this assumption ${}^{srf}G_m^{\phi}$ is expressed as:

$${}^{srf}G_m^{\phi} = \sum_i {}^{\circ}G_{end(i)}^{\phi} \prod_s y_{j(i)}^s \tag{4.13}$$

where each ${}^{\circ}G_{end(i)}^{\phi}$ represents an end-member and $y_{j(i)}^s$ is the site fraction of component j on sublattice s, that corresponds to the end-member i. As a component can be a constituent on several different sublattices it is here necessary to use site fractions (y_j) instead of mole fractions (x_j). Consequently is also the configurational entropy (${}^{conf}S_m^{\phi}$) within CEF expressed using y:

$${}^{conf}S_m^{\phi} = -R \sum_s \sum_j a_s y_j^s ln y_j^s \tag{4.14}$$

where a_s is the number of sites on sublattice s. Furthermore, the molar excess Gibbs energy contribution (${}^{E}G_m^{\phi}$) can be expressed as:

$${}^{E}G_m^{\phi} = \sum_i \left(I_i \prod y_{j(i)}^s \right) \tag{4.15}$$

where each I_i is an interaction parameter and the $y^s_{j(i)}$ are the corresponding site fractions to each I_i. As a simple example would ${}^{E}G^{\phi}_{m}$ for the hypothetical $(A, B, C)_a(D)_b$ system be:

$${}^{E}G^{\phi}_{m} = y'_A y'_B y''_D I_{A,B:D} + y'_A y'_C y''_D I_{A,C:D} + y'_B y'_C y''_D I_{B,C:D} + y'_A y'_B y'_C y''_D I_{A,B,C:D} \tag{4.16}$$

where the notations $'$ and $''$ are added in order to clarify if the y_j belongs to the first or second sublattice, respectively. Similar to the substitutional solution phases (Sec. 4.2), each I_i can then be modelled with a Redlich-Kister polynomial [55] (similar to Eq. 4.6), which can then also include T dependence (similar to Eq. 4.7). Many more examples of CEF can be found for the C-Cr-Ti system in **Paper III**, where all solid phases, except graphite, where modelled using CEF.

In the example above (Eq. 4.16), there is only interaction on one sublattice at a time. However, sometimes it is also necessary to use a parameter which models interactions on two sublattices simultaneously, e.g. $I_{A,B:C,D}$, where A and B are constituents on the first sublattice and C and D are constituents on the second sublattice. These type of parameters are called reciprocal interaction parameters. Their composition dependence cannot be explained with a Redlich-Kister polynomial [55], but are instead modelled as:

$$I^{\phi}_{A,B:C,D} = {}^{0}L^{\phi}_{A,B:C,D} + (y''_C - y''_D){}^{1}L^{\phi}_{A,B:C,D} + (y'_A - y'_B)^2 L^{\phi}_{A,B:C,D} \tag{4.17}$$

where each ${}^{i}L^{\phi}_{A,B:C,D}$ can include T dependence (similar to Eq. 4.7). This type of reciprocal interaction parameter was used for the fcc phase in the thermodynamic assessment of the C-Cr-TI system (**Paper III**).

It can be difficult to imagine how the different interaction parameters (L) contributes to $G^{\phi}_{m}(T)$, why it can be a good idea to try to visualize this. Fig. 4.1 shows an attempt to do this, at an arbitrary T, for the hypothetical $(A,B)_1(C,D)_1$ system. ${}^{srf}G^{\phi}_{m}(T)$ (the grid) and $G^{\phi}_{m}(T)$ for an ideal solution (the surface) are plotted and the different $L's$ are labelled to show at what compositions they affect $G^{\phi}_{m}(T)$. As this figure also show, ${}^{srf}G^{\phi}_{m}(T)$ does not necessarily have to be flat, even if all its edges have to be linear, i.e. the line of reference for each binary is linear.

4.4 Metastable elements and compounds

For metastable or unstable elements and compounds, adequate experimental information is not available, why other methods are needed. One way is to use DFT to calculate ${}^{\circ}G^{\phi}_{m}(T)$ (Sec. 3) which for example were used for several allotropes of Fe, Co and Ni in **Paper II**, for fcc-CrC in **Paper III** and for hcp-Cr_2C in **Paper IV**. The DFT calculated ${}^{\circ}G^{\phi}_{m}(T)$ can then still be fitted to either the second (Eq. 4.2) or the third generation model (Eq. 4.3). However, if also DFT calculated ${}^{\circ}G^{\phi}_{m}(T)$ values are unavailable, ${}^{\circ}G^{\phi}_{m}(T)$ has to be estimated in another way since descriptions of all end-members are required. One method can then be to use extrapolation from stable compositions of the phase. An alternative for compounds

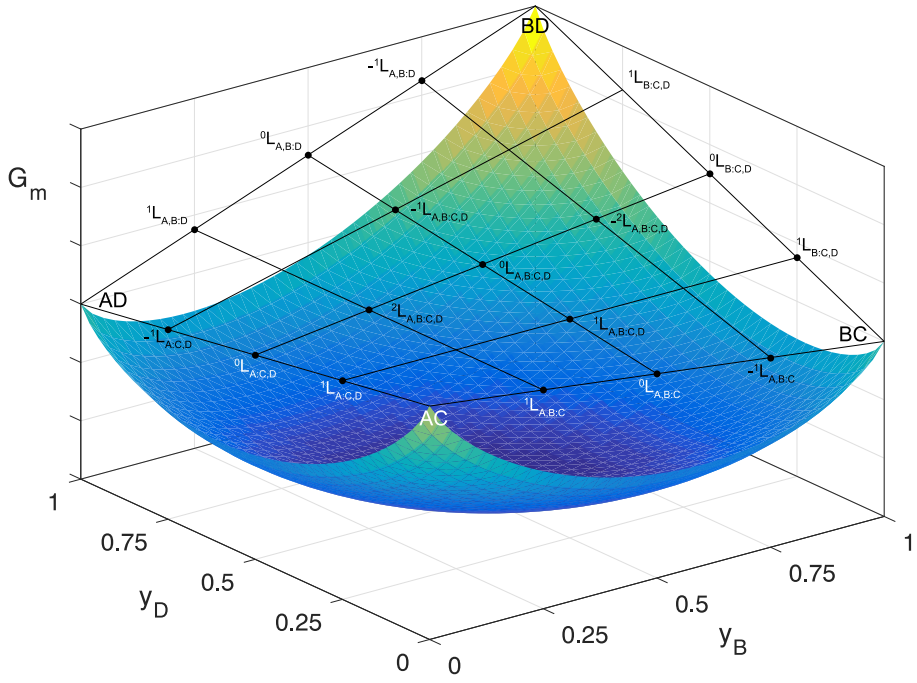

Figure 4.1: Schematic figure of the reciprocal $(A,B)_1(C,D)_1$ system. The grid represents the surface of reference (${}^{srf}G_m^{\phi}(T)$). The "hanging sheet" represents $G_m^{\phi}(T)$ for an ideal solution, i.e ${}^{srf}G_m^{\phi}(T) + {}^{conf}G_m^{\phi}(T)$. Finally, the different interaction parameters (L) are labelled on the grid to show at which compositions they affect $G_m^{\phi}(T)$. A positive value of L means that the sheet ($G_m^{\phi}(T)$) is "pulled" upwards at this position. However, for the $L's$ with a minus (-) in front of them it is the opposite.

is also to use the Neumann-Kopp rule, which for example has been described by Hillert [51]. The Neumann-Kopp rule is a linear combination of the isobaric heat capacities ($C_P(T)$) of the components. However, in CALPHAD one often takes a linear combination of ${}^{\circ}G_m^{\phi}(T)$ for the components and adjust the A+BT term:

$$ {}^{\circ}G_m^{\phi}(T) - \sum_i a_i H_i^{SER} = \sum_i a_i {}^{\circ}G_i^{SER} + A + BT \tag{4.18} $$

4.5 Magnetic contribution to Gibbs energy

As described in Sec. 3.6, several transition metal compounds undergoes a magnetic transition at some critical temperature (T_C or T_N). The transition type is of the second order, which means that it results in a discontinuity in the second

order derivative of $G_m^\phi(T)$ (i.e. in $C_P(T)$), but there is no discontinuity in the first derivative of $G_m^\phi(T)$ (i.e. $S_m^\phi(T)$), which it is for first order transitions, e.g. chemical phase transitions as bcc $\rightarrow$ fcc. The reason why the magnetic transition type is of the second order is due to magnetic short range ordering in the structure at temperatures close to the transition T, i.e. the transition is not distinct but gradual. This makes it problematic to treat the ordered magnetic state (FM or AFM) and the PM state as two different phases, why an empirical magnetic model has been developed within the CALPHAD community through the years. The first version was presented by Inden [61]. The model was then simplified by Hillert and Jarl [62] and finally the model parameters were refined by Chen and Sundman [52]. With this model the total $G_m^\phi(T)$ for an end-member can be calculated as:

$$G_m^\phi(T) = {}^{PM}G_m^\phi(T) + {}^{mo}G_m^\phi(T) \tag{4.19}$$

where the purpose of the added magnetic ordering contribution (${}^{mo}G_m^\phi(T)$ is that $G_m^\phi(T)$ should represent ${}^{FM}G_m^\phi(T)$ at temperatures below T_C. Fig. 4.2 shows a schematic figure of how ${}^{FM}G_m^\phi(T)$, ${}^{PM}G_m^\phi(T)$ and $G_m^\phi(T)$ are related with this magnetic model. As described by Chen and Sundman [52], ${}^{mo}G_m^\phi(T)$ can be expressed as:

$${}^{mo}G_m^\phi(T) = RTln(\beta+1)f(\tau) \tag{4.20}$$

where β is the average magnetic moment per atom and $\tau = T/T_C$.
For $\tau \leq 1$, $f(\tau)$ is:

$$\begin{aligned} f(\tau) = 1 - \Bigg[0.38438376\frac{\tau^{-1}}{p} + 0.63570895\left(\frac{1}{p}-1\right) \\ \times \left(\frac{\tau^3}{6} + \frac{\tau^9}{135} + \frac{\tau^{15}}{600} + \frac{\tau^{21}}{1617}\right)\Bigg] \Big/ D \end{aligned} \tag{4.21}$$

and for $\tau > 1$, $f(\tau)$ is:

$$f(\tau) = -\left(\frac{\tau^{-7}}{21} + \frac{\tau^{-21}}{630} + \frac{\tau^{-35}}{2975} + \frac{\tau^{-49}}{8232}\right) \Big/ D \tag{4.22}$$

where D is a constant, dependent on a structure factor (p), as:

$$D = 0.33471979 + 0.49649686\left(\frac{1}{p}-1\right) \tag{4.23}$$

The refined p values by Chen and Sundman [52] are p=0.37 for bcc-structures and p=0.25 for fcc- and hcp-structures.

However, in some cases it is better to use ${}^{FM}G_m^\phi(T)$ as reference instead and add a magnetic disordering contribution (${}^{mdo}G_m^\phi(T)$), in order to describe the transition to the PM structure above T_C:

$$G_m^\phi(T) = {}^{FM}G_m^\phi(T) + {}^{mdo}G_m^\phi(T) \tag{4.24}$$

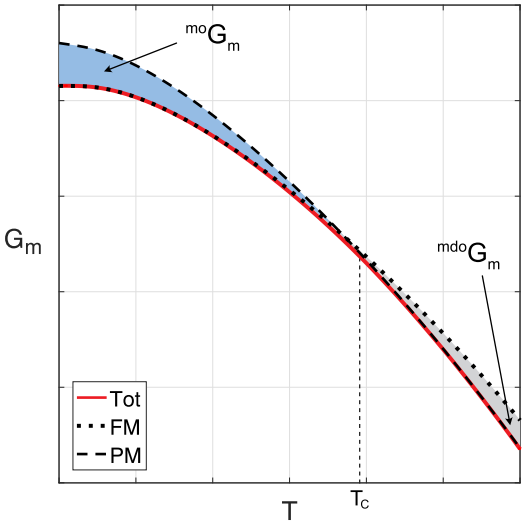

Figure 4.2: Schematic figure showing how ${}^{FM}G_m^{\phi}(T)$ (dotted line), ${}^{PM}G_m^{\phi}(T)$ (dashed line), $G_m^{\phi}(T)$ (solid red line), ${}^{mo}G_m^{\phi}(T)$ (blue area), ${}^{mdo}G_m^{\phi}(T)$ (grey area) and T_C are related in the Inden, Hillert and Jarl magnetic model [52,61,62], which often is used in CALPHAD descriptions.

One example when this is useful is when ${}^{FM}G_m^{\phi}(T)$ is calculated using DFT, as in **Paper II**. Another example can be if there is experimental information available for the FM state but not for the PM state. According to Chen and Sundman [52], ${}^{mdo}G_m^{\phi}(T)$ can be expressed as a function of ${}^{mo}G_m^{\phi}(T)$ as:

$$ {}^{mdo}G_m^{\phi}(T) = {}^{mdo(\infty)}G_m^{\phi}(T) + {}^{mo}G_m^{\phi}(T) \tag{4.25} $$

where ${}^{mdo(\infty)}G_m^{\phi}(T)$ is:

$$ {}^{mdo(\infty)}G_m^{\phi}(T) = -Rln(\beta+1)\left(T - 0.38438376\frac{T_C}{pD}\right) \tag{4.26} $$

The total $G_m^{\phi}(T)$ can then be expressed as:

$$ G_m^{\phi}(T) = {}^{FM}G_m^{\phi}(T) + {}^{mdo(\infty)}G_m^{\phi}(T) + {}^{mo}G_m^{\phi}(T) \tag{4.27} $$

The above described model (IHJ) was originally developed for FM materials. However it is also applicable to AFM structures, by just replacing T_C with T_N.

In a CALPHAD description it is necessary to describe, not only stable, but also metastable and unstable phases. A typical example is if element A is stable as fcc and element B is stable as bcc. To model the A-B system correctly and to

be able to predict the phase transitions between bcc and fcc in this system, also the metastable bcc-A and fcc-B end-members have to be described. Analogously, for magnetic phases this means that if element C is FM and element D is AFM, then also AFM C and FM D have to be described. However, it is not trivial to estimate β and T_C/T_N, for the metastable magnetic configuration of a phase. For example, Hertzman and Sundman [63] solved this for the Fe-Cr system by introducing the Weiss factor (W_f), which relates T_N to T_C as T_N=T_C/W_f, where commonly $W_f = -1$ for bcc and $W_f = -3$ for fcc and hcp. Also the average magnetic moments per atom (β) are related in the same way. This concept has then been widely used for the IHJ model. However, this approximation does not work for all systems and therefore Xiong et al. [64] proposed that T_N and T_C for a phase should be independent and used two separate Redlich-Kister polynomials [55]. Fig. 4.3 shows an example from **Paper IV**, where the magnetic properties as a function of N content in fcc (CrC−CrN) have been calculated using DFT. As these figures show, only the model proposed by Xiong et al. [64] (IHX) (Fig. 4.3b) is capable of describing both the stable and metastable magnetic properties correctly. The model by Hertzman and Sundman [63] (IHJ) is unable to do this because T_N (red curve in 4.3a) is simply T_C (black curve in 4.3a) divided by -3 (W_f). This is not important for this interaction, as only the stable magnetic properties are accounted for and negative T_C/T_N values are neglected, in both models. However, it is important for extrapolations to higher order systems, where all values, positive or negative, are used as end-points for the extrapolations and will therefore affect at what composition a system turns magnetic.

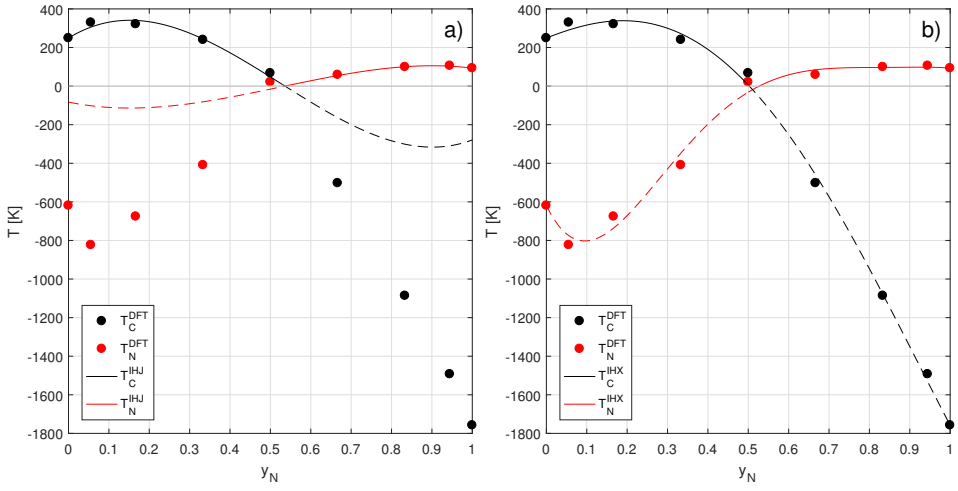

Figure 4.3: Example from **Paper IV**. T_C and T_N as a function of N content for fcc-Cr(C,N). Markers show DFT calculated values, which then are described with interaction parameters of Redlich-Kister type [55] (similar to Eq. 4.6) using the magnetic models a) IHJ [61–63] and b) IHX [64].

Chapter 5

Summary of the included papers

5.1 Paper I - Experimental study of carbides in the Ti–Cr–C system

Paper I presents an experimental study of carbides in the C-Cr-Ti system at 1673 and 1773 K. The solubility limits of these carbides are important, especially for cemented carbides and are crucial in order to be able to predict the stable phases in a designed cemented carbide grade containing Ti and Cr. Previous work on this topic present deviating results, probably due to different heat treatment times of the samples. In the experiments for this paper, much longer heat treatment times and different sets of raw materials are used to ensure that equilibrium is reached and XRD together with Rietveld refinement is used to verify the EDS/WDS measurements.

5.2 Paper II - CALPHAD: Method for calculation of finite temperature thermodynamic properties for magnetic allotropes — Case study on Fe, Co and Ni

Paper II presents a developed method for calculation of magnetic and finite temperature thermodynamic properties for stable, metastable and dynamically unstable allotropes. For CALPHAD descriptions, the possibility to make reliable estimations of these properties are very important, especially for metastable- and dynamically unstable allotropes where experimental information often is missing. Previous work on this topic are focusing on stable magnetic allotropes and/or only a part of the temperature interval (e.g. the paramagnetic part). The developed method is first used to estimate the magnetic transition temperature (T_C or T_N) and then to calculate finite temperature thermodynamic properties from 0 K up to approximately the melting temperature for the bcc, fcc and hcp allotropes of Fe, Co and Ni. Finally, the results are compared with existing thermodynamic descriptions of these allotropes.

5.3 Paper III - Thermodynamic assessment of the C-Cr-Ti system — Supported by DFT calculations

Paper III presents a thermodynamic reassessment of the C-Cr-Ti system. In the cemented carbide industry, especially, but also in the steel industry, the elements C, Cr and Ti are very important. Therefore an updated thermodynamic description of this ternary system is necessary. Since the previous thermodynamic description of this system by Schuster and Du [5] was published, all the three constituent binary systems have been updated. Furthermore, the new experiments from **Paper I** showed that the previous description does not correctly reproduce the solubility of Cr in MC (M=Cr, Ti), and also does not consider the measured solubility of Ti in M_3C_2 and M_7C_3. In this paper (**Paper III**) a critical review is made of published thermodynamic descriptions of the three constituent binary systems. Gibbs energy descriptions of crucial metastable end-members are calculated with the method developed in **Paper II** to ensure more reliable predictions at low temperatures. Finally, model parameters are assessed to reproduce both previously, and recently, published experimental information found in literature.

5.4 Paper IV - DFT study of the C-Cr-N system

Paper IV presents a computational study of the C-Cr-N system. The method developed in **Paper II** is first used to calculate $G_m(T)$ for the stable compounds fcc-CrN and hcp-Cr_2N, in order to further verify the method. The method is then used to calculate $G_m(T)$ for the metastable compound hcp-Cr_2C, and the molar excess Gibbs energy as a function of N content in fcc-Cr(C,N) and hcp-Cr_2(C,N). Also T_C and T_N as a function of composition are both calculated for the same composition range and the possibility to fit these results with the magnetic models by Inden-Hillert-Jarl (IHJ) [61, 62] and Xiong et al. [64] are discussed. Calculated results are compared with existing thermodynamic descriptions of these parameters.

Chapter 6

Concluding remarks

In this thesis the CALPHAD method has been used to study transition metals and their carbides, nitrides, and carbonitrides. All three parts of CALPHAD, experiments, computational methods and thermodynamic modelling, were used and below follows the main outcomes:

1. The solubility of Cr in MC (M = Ti, Cr) and of Ti in M_3C_2 and M_7C_3, in the C-Cr-Ti system, were determined by performing experiments at 1673 and 1773 K in the equilibria MC-M_3C_2-M_7C_3 and MC-M_3C_2-graphite. The solubilities were measured with EDS/WDS and verified with XRD/Rietveld refinement.

2. A computational method for calculation of $G_m(T)$ and $C_P(T)$ for metastable magnetic compounds was developed. However, the method can of course also be used on stable and/or non-magnetic compounds. The method uses DFT in combination with the Debye-Grüneisen model and the magnetic model implemented in CALPHAD. The developed method is also able to estimate the magnetic transition temperature (T_C or T_N). Two new approaches for how to treat calculations on dynamically unstable allotropes were also developed, which often is the reason why DFT calculations for metastable compounds fail. The method was developed and verified on bcc, fcc and hcp allotropes of Fe, Co and Ni, but was then also used to calculate $G_m(T)$ descriptions for fcc-TiC, fcc-CrC, fcc-CrN, hcp-Cr_2C and hcp-Cr_2N. The developed method was also used to calculate the excess Gibbs energy at 0 K for the interactions CrC-TiC (fcc), CrC-CrN (fcc) and Cr_2C-Cr_2N (hcp), as well as T_C and T_N as a function of composition for the same sections.

3. Thermodynamic modelling was used to perform a reassessment of the C-Cr-Ti system. Compared to the previous thermodynamic description by Schuster and Du [5], the new description includes updated descriptions for two of the three constituent binary systems (C-Ti [65] and Cr-Ti [66]). It also reproduces the experimental information of the solubility of Cr in MC (M = Ti, Cr) and

of Ti in M_3C_2 and M_7C_3 from this thesis work, as well as experimental results in the TiC-Cr_3C_2 isoplethal section by Carter [67]. Furthermore, it uses descriptions of important metastable end-members and interaction parameters calculated with the developed method in this thesis work, which gives more reliable predictions at low T.

Finally, the topic of this thesis is very broad, and only a very limited part of the subject has been investigated. However, the techniques and models used within this thesis are general. Both the well proven ones as EDS, WDS, XRD, DFT and the CALPHAD method, but also the new method for calculation of $G_m(T)$ for metastable magnetic compounds. This method can thus be a useful tool for calculation of $G_m(T)$ for many other transition metals and their carbides, nitrides, and carbonitrides, in the future.

Chapter 7

Suggestions for future work

7.1 C-Cr-N system

The natural continuation of this work is to perform equilibrium experiments in the C-Cr-N system, which then together with the computational results from **Paper IV**, can be the base for a thermodynamic assessment of this system. The existing thermodynamic description of the C-Cr-N system [68] is based on experimental information at only one temperature [11]. This can also explain why the assessed interaction parameters for fcc-Cr(C,N) and hcp-Cr_2(C,N) are constants, i.e. without temperature dependence. This means that they should represent the interaction at 0 K, but according to the calculations in **Paper IV** the values are not correct. With both information at 0 K from the calculations and at higher temperature from experiments it would be possible to fit these interaction parameters with an A+BT term, which would result in a better description for the whole temperature range.

Another issue is the interaction parameters for fcc-Cr_2(N,Va) and hcp-Cr_2(N,Va) in the Cr-N system by Frisk [10], and especially for hcp which is known to be substoichiometric and able to include a lot of vacancies (Va) in the second sublattice. These parameters are important in order to correctly describe the solubility limit of C in fcc-Cr(C,N) and hcp-Cr_2(C,N). To retrieve better descriptions for these parameters over the whole temperature range, it would therefore be interesting to calculate these parameters in a similar way as the interaction parameters for fcc-Cr(C,N) and hcp-Cr_2(C,N) in **Paper IV**.

7.2 Method development

The method developed in **Paper II** for calculation of $G_m(T)$ and $C_P(T)$ for metastable magnetic allotropes, which then were used also for compounds in **Paper III** and **IV**, has been shown to work well in general. However, there are some deviations and especially the calculated $C_P(T)$ increases drastically for some struc-

tures at higher T, as Fig. 7.1 shows. To some extent this might be an effect of that anharmonic contributions have been neglected. However, another more reasonable explanation is that the $E-V$ curve for the ordered magnetic state (FM or AFM) is used as input to the Debye-Grüneisen model (Sec. 3.3). The quasi-harmonic approximation is therefore made with this structure, and then the PM state is calculated by adding a magnetic disordering contribution (Sec. 4.5). This means that when the FM (or AFM) structure collapse at high T, where it is metastable, e.g. as it does for bcc-Fe above $\approx$ 1300 K, the developed method no longer works.

The most correct approach would be to calculate $G_m(T)$ for both the ordered magnetic state and the PM state separately, and then try to fit the magnetic model (Sec. 4.5) to these two $G_m(T)$ descriptions. However, in order to retrieve θ_D for the PM state, this would require to perform harmonic phonon calculations on the DLM-SQS supercell, which is extremely time consuming. An alternative could be to assume that θ_D for the PM structure is equal to θ_D for the ordered structure, but to use different $E-V$ curves to calculate $G_m(T)$ for each state.

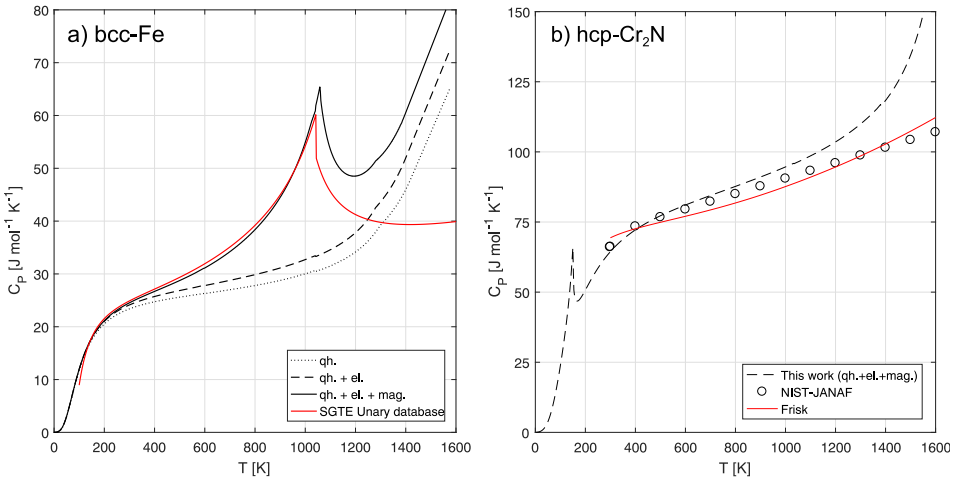

Figure 7.1: Examples from **Paper II** and **IV**. Calculated $C_P(T)$ for a) bcc-Fe and b) hcp-Cr_2N. Quasi-harmonic- (qh.), electronic- (el.) and magnetic- (mag.) contributions are calculated in this thesis work. Results are compared with the SGTE Unary database [69] and Frisk [10].

Chapter 8

The 17 sustainable development goals

In 2015, world leaders agreed on 17 global goals for a sustainable development [70] (Fig. 8.1). The target is to create a better world by 2030, but in order to achieve these goals everybody has to contribute. KTH actively work on this topic and in this chapter I will explain how this thesis work contributes to some of these 17 global goals (Fig. 8.1).

Figure 8.1: The 17 global goals for sustainable development.

Paper I - *Experimental study of carbides in the Ti–Cr–C system*, and **Paper III -** *Thermodynamic assessment of the C−Cr−Ti system − Supported by DFT calculations*, contributes to an increased knowledge about the C-Cr-Ti system. In a similar way, **Paper IV -** *DFT study of the C−Cr−N system* contributes to an increased knowledge about the C-Cr-N system. This improves the possibility for process- and product developments where C, Cr, N and Ti are essential elements, e.g. in the cemented carbide and steel industries. At the end, this leads to improved products and processes and the needed number of a real trials will be reduced.

Paper II - *CALPHAD: Method for calculation of finite temperature thermodynamic properties for magnetic allotropes - Case study on Fe, Co and Ni*, provides an increased possibility, using DFT, to calculate Gibbs energy as a function of temperature for metastable phases, and in particular for metastable magnetic phases. This gives the opportunity to more accurately describe parts of CALPHAD descriptions that cannot be verified experimentally. In the extension, this provides improved descriptions and the ability to perform thermodynamic calculations with greater precision. Ultimately, the need for the number of real trials is reduced.

Translated to the 17 global goals for a sustainable development [70], this thesis work will mainly contribute to the following four goals:

7. **Affordable and clean energy** − Calculations instead of real trials contributes to reduced energy consumption.

9. **Industry, innovation and infrastructure** − Improved CALPHAD descriptions contributes to a sustainable industry by improved possibilities to find new innovative solutions, e.g. in the cemented carbide industry. Both in the development of new products, but also in the development of the manufacturing processes.

12. **Responsible consumption and production** − Improved products/processes and reduced number of needed real trials contributes to a reduced amount of needed raw materials, which means a more sustainable consumption and production.

13. **Climate action** − Improved products/processes and reduced number of needed real trials contributes to a reduced amount of needed raw materials and a reduced energy consumption.

References

[1] N. Saunders and A. Miodownik, *CALPHAD (Calculation of Phase Diagrams): A Comprehensive Guide*, vol. 1. Pergamon, 1998.

[2] H. Lukas, S. Fries, and B. Sundman, *Computational thermodynamics: the Calphad method*. Cambridge university press New York, 2007.

[3] Z. He, "CALPHAD study of cubic carbide systems with Cr," *Master thesis*, vol. diva2:862092, 2015.

[4] A. Ehrenborg, "Investigation of the Cr solubility in the MC phase," *Master thesis*, vol. diva2:921311, 2016.

[5] J. Schuster and Y. Du, "Thermodynamic description of the system Ti-Cr-C," *Calphad*, vol. 23, no. 3, pp. 393 – 408, 1999.

[6] P. Booker, A. Kunrath, and M. Hepworth, "Experimental determination of the ternary diagram of the Ti-Cr-C system," *Acta Materialia*, vol. 45, no. 4, pp. 1625–1632, 1997.

[7] K. K. Kelley, "Specific heats at low temperatures of titanium and titanium carbide," *Industrial & Engineering Chemistry*, vol. 36, no. 9, pp. 865–866, 1944.

[8] L. S. Levinson, "High-Temperature Heat Contents of TiC and ZrC," *The Journal of Chemical Physics*, vol. 42, no. 8, pp. 2891–2892, 1965.

[9] T. Mills, "Pressure-temperature relations in the chromium-nitrogen system," *Journal of the Less Common Metals*, vol. 22, no. 4, pp. 373–381, 1970.

[10] K. Frisk, "A thermodynamic evaluation of the Cr-N, Fe-N, Mo-N and Cr-Mo-N systems," *Calphad*, vol. 15, no. 1, pp. 79–106, 1991.

[11] S. Hertzman, "An experimental and thermodynamic analysis of the Fe-Cr-C-N system at 1000 °C," *Trita-MAC-0242*, 1984.

[12] H. M. Rietveld, "A profile refinement method for nuclear and magnetic structures," *Journal of Applied Crystallography*, vol. 2, no. 2, pp. 65–71, 1969.

[13] J. I. Goldstein, D. E. Newbury, P. Echlin, D. C. Joy, C. E. Lyman, E. Lifshin, L. Sawyer, and J. R. Michael, *Scanning Electron Microscopy and X-ray Microanalysis*. Springer, Boston, MA, 3rd ed., 2003.

[14] L. Vegard, "Die konstitution der mischkristalle und die raumfüllung der atome," *Zeitschrift für Physik*, vol. 5, pp. 17–26, Jan 1921.

[15] C. Suryanarayana and M. G. Norton, *X-Ray Diffraction A Practical Approach*. Springer Science+Business Media New York, 1998.

[16] U. Gonser, C. Meechan, A. Muir, and H. Wiedersich, "Determination of Néel temperatures in fcc iron," *J. of Appl. Phys.*, vol. 34, no. 8, pp. 2373–2378, 1963.

[17] C. S. Tian, D. Qian, D. Wu, R. H. He, Y. Z. Wu, W. X. Tang, L. F. Yin, Y. S. Shi, G. S. Dong, X. F. Jin, X. M. Jiang, F. Q. Liu, H. J. Qian, K. Sun, L. M. Wang, G. Rossi, Z. Q. Qiu, and J. Shi, "Body-centered-cubic ni and its magnetic properties," *Phys. Rev. Lett.*, vol. 94, p. 137210, Apr 2005.

[18] H. Ohno, "Antiferromagnetism in hcp iron-ruthenium and hcp iron-osmium alloys," *J. of the Phys. Soc. of Jpn.*, vol. 31, no. 1, pp. 92–101, 1971.

[19] P. Debye, "Zur Theorie der spezifischen Wärmen," *Annalen der Phys.*, vol. 344, no. 14, pp. 789–839, 1912.

[20] E. Grüneisen, "Theorie des festen Zustandes einatomiger Elemente," *Annalen der Phys.*, pp. 257–306, Jan. 1912.

[21] M. Born and R. Oppenheimer, "Zur quantentheorie der molekeln," *Annalen der Physik*, vol. 389, no. 20, pp. 457–484, 1927.

[22] P. Hohenberg and W. Kohn, "Inhomogeneous electron gas," *Phys. Rev.*, vol. 136, pp. B864–B871, Nov 1964.

[23] W. Kohn and L. J. Sham, "Self-consistent equations including exchange and correlation effects," *Phys. Rev.*, vol. 140, pp. A1133–A1138, Nov 1965.

[24] G. Kresse and J. Furthmüller, "Efficiency of ab-initio total energy calculations for metals and semiconductors using a plane-wave basis set," *Comp. Mat. Sci.*, vol. 6, no. 1, pp. 15–50, 1996.

[25] G. Kresse and J. Furthmüller, "Efficient iterative schemes for ab initio total-energy calculations using a plane-wave basis set," *Phys. Rev. B*, vol. 54, pp. 11169–11186, Oct 1996.

[26] P. E. Blöchl, "Projector augmented-wave method," *Phys. Rev. B*, vol. 50, pp. 17953–17979, Dec 1994.

[27] G. Kresse and D. Joubert, "From ultrasoft pseudopotentials to the projector augmented-wave method," *Phys. Rev. B*, vol. 59, pp. 1758–1775, Jan 1999.

[28] J. P. Perdew, K. Burke, and M. Ernzerhof, "Generalized Gradient Approximation Made Simple," *Phys. Rev. Lett.*, vol. 77, pp. 3865–3868, Oct 1996.

[29] A. Togo and I. Tanaka, "First principles phonon calculations in materials science," *Scr. Mater.*, vol. 108, pp. 1 – 5, 2015.

[30] K. Parlinski, Z. Q. Li, and Y. Kawazoe, "First-principles determination of the soft mode in cubic ZrO_2," *Phys. Rev. Lett.*, vol. 78, pp. 4063–4066, May 1997.

[31] F. Birch, "Finite elastic strain of cubic crystals," *Phys. Rev.*, vol. 71, pp. 809–824, Jun 1947.

[32] F. D. Murnaghan, "The compressibility of media under extreme pressures," *Proc. of the Natl. Academy of Sci.*, vol. 30, no. 9, pp. 244–247, 1944.

[33] V. L. Moruzzi, J. F. Janak, and K. Schwarz, "Calculated thermal properties of metals," *Phys. Rev. B*, vol. 37, pp. 790–799, Jan 1988.

[34] Q. Chen and B. Sundman, "Calculation of debye temperature for crystalline structures—a case study on Ti, Zr, and Hf," *Acta Mater.*, vol. 49, no. 6, pp. 947 – 961, 2001.

[35] X. Gonze and C. Lee, "Dynamical matrices, born effective charges, dielectric permittivity tensors, and interatomic force constants from density-functional perturbation theory," *Phys. Rev. B*, vol. 55, pp. 10355–10368, Apr 1997.

[36] V. N. Zharkov and V. A. Kalinin, *Equation of State for Solids at High Pressures and Temperatures*. Springer Science+Business Media New York, 1971.

[37] J. S. Dugdale and D. K. C. MacDonald, "The thermal expansion of solids," *Phys. Rev.*, vol. 89, pp. 832–834, Feb 1953.

[38] A. Glensk, B. Grabowski, T. Hickel, and J. Neugebauer, "Understanding anharmonicity in fcc materials: From its origin to ab initio strategies beyond the quasiharmonic approximation," *Phys. Rev. Lett.*, vol. 114, p. 195901, May 2015.

[39] B. Grabowski, L. Ismer, T. Hickel, and J. Neugebauer, "Ab initio up to the melting point: Anharmonicity and vacancies in aluminum," *Phys. Rev. B*, vol. 79, p. 134106, Apr 2009.

[40] S. Bigdeli, H. Ehteshami, Q. Chen, H. Mao, P. Korzhavy, and M. Selleby, "New description of metastable hcp phase for unaries Fe and Mn: Coupling between first-principles calculations and CALPHAD modeling," *Phys. Status Solidi (b)*, vol. 253, 05 2016.

[41] Y. Tsunoda, "Spin-density wave in cubic γ-Fe and γ-Fe100-xCoxprecipitates in Cu," *J. of Phys.: Condens. Matter*, vol. 1, pp. 10427–10438, dec 1989.

[42] E. Sjöstedt and L. Nordström, "Noncollinear full-potential studies of $\gamma - Fe$," *Phys. Rev. B*, vol. 66, p. 014447, Jul 2002.

[43] M. Marsman and J. Hafner, "Broken symmetries in the crystalline and magnetic structures of γ-iron," *Phys. Rev. B*, vol. 66, p. 224409, Dec 2002.

[44] L. M. Corliss, J. M. Hastings, and R. J. Weiss, "Antiphase antiferromagnetic structure of chromium," *Phys. Rev. Lett.*, vol. 3, pp. 211–212, Sep 1959.

[45] G. Grimvall, "Spin disorder in paramagnetic fcc iron," *Phys. Rev. B*, vol. 39, pp. 12300–12301, Jun 1989.

[46] A. Zunger, S.-H. Wei, L. G. Ferreira, and J. E. Bernard, "Special quasirandom structures," *Phys. Rev. Lett.*, vol. 65, pp. 353–356, Jul 1990.

[47] S.-H. Wei, L. G. Ferreira, J. E. Bernard, and A. Zunger, "Electronic properties of random alloys: Special quasirandom structures," *Phys. Rev. B*, vol. 42, pp. 9622–9649, Nov 1990.

[48] M. Ångqvist, W. A. Muñoz, J. M. Rahm, E. Fransson, C. Durniak, P. Rozyczko, T. H. Rod, and P. Erhart, "Icet – a python library for constructing and sampling alloy cluster expansions," *Advanced Theory and Simulations*, vol. 2, no. 7, p. 1900015, 2019.

[49] F. Körmann, A. Dick, B. Grabowski, T. Hickel, and J. Neugebauer, "Atomic forces at finite magnetic temperatures: Phonons in paramagnetic iron," *Phys. Rev. B*, vol. 85, p. 125104, Mar 2012.

[50] Z. Dong, W. Li, S. Schönecker, S. Lu, D. Chen, and L. Vitos, "Thermal spin fluctuation effect on the elastic constants of paramagnetic Fe from first principles," *Phys. Rev. B*, vol. 92, p. 224420, Dec 2015.

[51] M. Hillert, *Phase Equilibria, Phase Diagrams and Phase Transformations: Their Thermodynamic Basis*. Cambridge University Press, 2 ed., 2007.

[52] Q. Chen and B. Sundman, "Modeling of thermodynamic properties for bcc, fcc, liquid, and amorphous iron," *J. of Phase Equilibria*, vol. 22, pp. 631–644, Nov 2001.

[53] M. W. Chase, I. Ansara, A. Dinsdale, G. Eriksson, G. Grimvall, L. Höglund, and H. Yokokawa, "Workshop on thermodynamic models and data for pure elements and other endmembers of solutions: Schloß Ringberg, Feb. 26 to March 3, 1995," *Calphad*, vol. 19, no. 4, pp. 437 – 447, 1995.

[54] D. de Fontaine, S. G. Fries, G. Inden, P. Miodownik, R. Schmid-Fetzer, and S.-L. Chen, "Workshop on thermodynamic models and data for pure elements and other endmembers of solutions: Schloß Ringberg, Febr. 26, to March 3, 1995," *Calphad*, vol. 19, no. 4, pp. 499 – 536, 1995.

[55] O. Redlich and A. T. Kister, "Algebraic Representation of Thermodynamic Properties and the Classification of Solutions," *Industrial & Engineering Chemistry*, vol. 40, no. 2, pp. 345–348, 1948.

[56] M. Hillert, "Empirical methods of predicting and representing thermodynamic properties of ternary solution phases," *Calphad*, vol. 4, no. 1, pp. 1–12, 1980.

[57] M. Hillert and L.-I. Staffansson, "The regular solution model for stoichiometric phases and ionic melts," *Acta Chem. Scnad.*, vol. 24, pp. 3618–3626, 1970.

[58] H. Harvig, "An extended version of the regular solution model for stoichiometric phases and ionic melts," *Acta Chem. Scnad.*, vol. 25, pp. 3199–3204, 1971.

[59] B. Sundman and J. Ågren, "A regular solution model for phases with several components and sublattices, suitable for computer applications," *Journal of Physics and Chemistry of Solids*, vol. 42, no. 4, pp. 297–301, 1981.

[60] M. Hillert, "The compound energy formalism," *Journal of Alloys and Compounds*, vol. 320, no. 2, pp. 161–176, 2001. Materials Constitution and Thermochemistry. Examples of Methods, Measurements and Applications. In Memoriam Alan Prince.

[61] G. Inden, "Report on the project meeting calphad v, june 21-25," *Max-Planck Institute für Metallkunde, Düsseldorf, West Germany*, 1976.

[62] M. Hillert and M. Jarl, "A model for alloying in ferromagnetic metals," *Calphad*, vol. 2, no. 3, pp. 227 – 238, 1978.

[63] S. Hertzman and B. Sundman, "A thermodynamic analysis of the Fe-Cr system," *Calphad*, vol. 6, no. 1, pp. 67–80, 1982.

[64] W. Xiong, Q. Chen, P. A. Korzhavyi, and M. Selleby, "An improved magnetic model for thermodynamic modeling," *Calphad*, vol. 39, pp. 11–20, 2012.

[65] K. Frisk, "A revised thermodynamic description of the Ti–C system," *Calphad*, vol. 27, no. 4, pp. 367–373, 2003.

[66] G. Ghosh, "Thermodynamic and kinetic modeling of the Cr-Ti-V system," *Journal of Phase Equilibria*, vol. 23, pp. 310–328, 2002.

[67] A. Carter, "The Solid Solubility of Chromium Carbide, Cr_3C_2, in Titanium Carbide," *J. Inst. Metals*, vol. 83, 1955.

[68] P. Gustafson and A. Johansson, "A thermodynamic study on nitrogen alloyed steels," *Swedish Institute for Metals Research, Internal report*, 1990.

[69] A. Dinsdale, "SGTE data for pure elements," *Calphad*, vol. 15, no. 4, pp. 317 – 425, 1991.

[70] The Global Goals for Sustainable Development, https://www.globalgoals.org/